A NEW GEOMETRIC METRIC IN THE SPACE OF CURVES, AND APPLICATIONS TO TRACKING DEFORMING OBJECTS BY PREDICTION AND FILTERING

GANESH SUNDARAMOORTHI*, ANDREA MENNUCCI†, STEFANO SOATTO ‡, AND ANTHONY YEZZI §

Abstract. We define a novel metric on the space of closed planar curves which decomposes into three intuitive components. According to this metric centroid translations, scale changes and deformations are orthogonal, and the metric is also invariant with respect to reparameterizations of the curve. While earlier related Sobolev metrics for curves exhibit some general similarities to the novel metric proposed in this work, they lacked this important three-way orthogonal decomposition which has particular relevance for tracking in computer vision. Another positive property of this new metric is that the Riemannian structure that is induced on the space of curves is a smooth Riemannian manifold, which is isometric to a classical well-known manifold. As a consequence, geodesics and gradients of energies defined on the space can be computed using fast closed-form formulas, and this has obvious benefits in numerical applications.

The obtained Riemannian manifold of curves is ideal to address complex problems in computer vision; one such example is the tracking of highly deforming objects. Previous works have assumed that the object deformation is *smooth*, which is realistic for the tracking problem, but most have restricted the deformation to belong to a finite-dimensional group – such as affine motions – or to finitely-parameterized models. This is too restrictive for highly deforming objects such as the contour of a beating heart. We adopt the smoothness assumption implicit in previous work, but we lift the restriction to finite-dimensional motions/deformations. We define a dynamical model in this Riemannian manifold of curves, and use it to perform filtering and prediction to infer and extrapolate not just the pose (a finitely parameterized quantity) of an object, but its deformation (an infinite-dimensional quantity) as well. We illustrate these ideas using a simple first-order dynamical model, and show that it can be effective even on image sequences where existing methods fail.

1. Introduction. Shape theory is central in computer vision because shapes partially characterize objects in images. Shapes appear in two broad categories of applications:

- *shape optimization*, where we want to find the best shape according to a criterion; examples include image segmentation and object tracking; and
- *shape analysis*, where we study families of shapes for purposes of statistics, (automatic) cataloging, probabilistic modeling, etc.

In this paper, the *shapes* we focus on are represented by smoothly immersed planar curves[1] which constitute the boundaries of compact domains (representing the boundaries of physical objects projected into the imaging plane). As customary in the literature of *active contours* [23], we will somewhat abusively call these curves *embedded curves* in the rest of the paper. It should be noted that the *shape space* classically used in shape optimization (i.e., active contours) is more precisely identi-

*Computer Science Department, University of California Los Angeles - CA, USA (ganeshs@ucla.edu)

†Scuola Normale Superiore, Pisa, Italy (a.mennucci@sns.it)

‡Computer Science Department, University of California, Los Angeles - CA, USA (soatto@ucla.edu)

§School of Electrical & Computer Engineering, Georgia Institute of Technology, Atlanta - GA, USA (ayezzi@ece.gatech.edu)

[1] We note that all of the mathematical theory connected with the metric presented in this paper depends only upon the assumption of immersedness. The extra assumptions are needed only when pairing this theory together with various region based energies that are typically minimized in various computer vision applications, including the tracking applications demonstrated at the end of this paper. Such energies are defined only for curves which have a well defined interior/exterior which is not the case for all immersed curves.

fied as *the space of embedded curves, up to a choice of parameterization*, whereas in shape analysis the space is usually identified as *the space of embedded curves, up to rotation, translation, scaling and reparameterization*.

The usage of the space of curves as a *shape space* in applications has predated the proper mathematical study of this shape space by almost two decades. Historically, in the active contour literature, many authors [23, 4, 29, 25, 5, 16] have defined energy functionals on curves, whose minima represent the desired object(s). In more recent works [45, 62, 59, 7], the curve was considered to be a contour partitioning the image into statistically distinct regions. In all cases, the authors utilized the calculus of variations to derive curve evolutions to search for the minima of the energy, often referring to these evolutions as gradient flows. Calling the minimizing flows *gradient flows*, however, implies a certain Riemannian metric on the space of curves.

Modeling the space of curves as a Riemannian manifold has also obvious benefits in shape analysis: indeed the distance between curves can be used for clustering, the geodesic can be used to define the average of two shapes, and so on. However, recently [33, 58] observed that nearly all previous works on geometric active contours that derive *gradient flows* to minimize energies (i.e., shape optimization) imply a natural notion of Riemannian metric, given by a geometric version of the standard $\mathbb{L}^2$ inner product, which we will call H^0 in eqn. (3.1). Subsequently, [33, 57] have shown a surprising property: the H^0 Riemannian metric on the space of curves is not meaningful, since the "distance" between *any* two curves is zero. (This phenomena is an example of a more general property, indeed [34] prove that the Fubini-Study metric induces geodesic distance 0 in the nonlinear Grassmannian of all submanifolds of type M in a Riemannian manifold (N, g).)

This opened a new period of mathematical study, with the goal of finding a new metric in the space of curves, that would provide a well-founded model. Many models have been presented, usually to be used either in shape analysis or in shape optimization, but not both. The study of shapes as points on an infinite dimensional space has then been the subject of considerable interest, [35, 32]; models and theory have been presented in [8, 36, 1, 13, 61, 46, 56].

Going back to the shape optimization tasks, many papers contain methods and studies that show that the active contour paradigm is successful in addressing object detection/image segmentation. Those methods can be extended to visual tracking, that is, to temporally varying data; the extension typically involves two steps. One is to collect local statistics from a single image (e.g. intensity histograms, spatial and temporal regularized derivatives etc.) and use them to partition the image domain into regions that have homogeneous statistics [5, 25, 38, 7, 12, 42]. The other step is to incorporate a model of the temporal variation of the deforming object into the tracking algorithm. The simplest way to extend the active contour methodology to time-varying imagery is to use the contour estimated at time "t" as initialization for the same gradient-based optimization at time "$t + 1$" [7]. This approach implicitly assumes trivial dynamics ("constant position plus perturbation"), so its prediction would trail an object moving with constant speed with a constant error. Better dynamics ("constant velocity plus perturbation") have been developed both for parametric [2, 53, 21, 43] and geometric [44, 39, 22] active contour models, the latter implemented using level set methods [40]. While these methods can more accurately predict the *(affine) motion* of the object, their deformation model remains overly simplistic, as – on average – they assume no deformation. So, the prediction of the motion of a jelly fish would extrapolate its affine trajectory (position, orientation, scale and skew) but “freeze” its shape to the last observation. The dynamical model – and therefore the predictive ability of the tracking scheme – is restricted to the finite-dimensional portion of the actual object deformation.

Recent work has moved beyond the assumption of affine motion [11, 54]. In [11], the motion/deformation is described by a linear autoregressive model defined on combinations of distance functions given as a training set. The applicability of this method is therefore restricted by the availability of training data for every particular object class and its associated deformations. In [54], the authors use a small time-varying basis, which is finite-dimensional but goes beyond affine, to dynamically model local deformations of the contour. In [41], an optimal control approach is constructed to moderate between a model based on optical flow [20] and the results of image segmentation, which results in temporal consistency of the object when compared to frame-by-frame image segmentation. While the model (i.e., a transport equation) allows for deformations beyond affine, the model is defined on the entire domain of the image and therefore the model is not intrinsic to the geometry of the deforming object. A model that is restricted to the object is natural for tracking because typically the dynamics of the object of interest are less complex than the object plus background, which can have additional dynamics. Also, the model of [41] is tied to image measurements via optical flow and therefore may have problems in the case of noisy/corrupted image measurements or when the brightness constancy assumption does not hold. In [17], deformations that are not affine are considered by mapping views of a single 3D object to the 2-sphere (in $\mathbb{R}^3$), and a constant velocity model is constructed on the mapped space. The mapping limits the shapes to projections from different viewpoints of the chosen 3D object, and moreover, the approach assumes that the underlying 3D object being viewed is rigid.

1.1. Paper Contributions. In the first part of the present work, we construct a Riemannian structure on the space of curves using a geometric-type Sobolev metric, which will be presented in Definition 3.1. While this metric will resemble some prior geometric Sobolev-type metrics for curves, it will exhibit a deliberate modification which was imposed to yield a special three-fold orthogonal decomposition (Theorem 3.4) chosen specifically for its usefulness in visual tracking applications. We present the relevant properties, and the formulas and methods to compute geodesics, parallel transport, and gradients of energies defined on curves according to this specialized metric. We show that, using our metric, all these operations can be numerically computed using fast algorithms. This metric builds on the experience of previous examples of Sobolev metrics [60, 35, 51, 61]; in particular, it extends the ideas found in [61] to the space of all embedded curves, so that this Riemannian metric can be used to address problems in shape analysis and shape optimization, and any desired combination of the two.

A Riemannian structure on the space of embedded curves, we show, also provides the means for constructing *dynamical systems on curves*, which is useful for modeling the dynamics of deforming objects. To illustrate these ideas, in the second part of the paper we consider the task of tracking highly deforming objects, such as a walking human, a maneuvering vehicle, a moving animal etc., from time-varying images. We are interested in the changes of *shape* induced by motion on the boundaries of the projection of objects of interest onto an image. For instance, the silhouette of a walking person undergoes complex deformations, including changes of topology as gaps open between limbs and the trunk. We wish to not only predict the coarse motion or pose of the boundary curves, but also to extrapolate their deformation [2]. To this end, we present a simple (infinite-dimensional) constant-velocity dynamical model of the contour, and then derive an associated filter that predicts and estimates the contour and its deformation based on local image statistics. For simplicity, in this work we consider intensity statistics, but local spatio-temporal filters could be used as well. Note that [52] considers tracking, however, but does not perform prediction and estimation, which is one of the main contributions of the present work.

One benefit in using Sobolev–type metrics in tracking is that they favor *smooth* motions of the curve without restricting its deformation [51]. The metric studied in [51], however, did not allow for an efficient computation of geodesics, whereas the new metric presented in this paper allows for efficient calculation of geodesics.

It must be noted that, one sure way to avoid infinite-dimensional Riemannian geometry (and the pathologies associated with some metrics) is to model the shape space as a *finite dimensional manifold*: such is the case for example in the work of Kendall [24] (some recent works include, e.g. [26, 3]). It is certainly possible to model curves using a finite dimensional family of parameters, for example using splines. This modeling though introduces later problems in tracking applications, since the motion of control points along the curve has to be factored out of the shape dynamics. Moreover, such finite-dimensional representations restrict the space of allowable deformations, which could have detrimental effects when tracking highly deforming objects. In this paper, we propose a tracking method where we define a dynamical model *directly* on the infinite-dimensional space of curves (allowing any smooth deformation), so as to model the deformation of the object of interest in a way that is natural with respect to the object's geometry.

A preliminary conference version of this paper has appeared in [48]. The current version gives detailed mathematical proofs and computations of the statements in the conference version. In Section C, we have added a new gradient descent procedure for the image segmentation that now corresponds with the new Sobolev metric presented in Section 3. We have also added a new experiment testing the approach on MRI data. A forthcoming paper will contain more mathematical analysis of the Riemannian metric presented in Definition 3.1.

2. Geometry in the Space of Curves.

We define the space of **smooth planar immersed curves** as

$$M = \{c \in C^\infty(\mathbb{S}^1, \mathbb{R}^2) : |c'(\theta)| \neq 0 \, \forall \theta \in \mathbb{S}^1\} \tag{2.1}$$

where $\mathbb{S}^1$ is the circle, and $c'(\theta)$ is the usual parametric derivative of c. The tangent space $T_c M$ at c is the set of vector fields h on c, i.e., $h : \mathbb{S}^1 \to \mathbb{R}^2$, which represent *infinitesimal deformations* of c.

We will endow M with a Riemannian metric $\|h\|_c$ which we will then use to define distances between curves in M, geodesics (i.e., shortest paths), the exponential map, and all other standard tools that are found in common texts on Riemannian Geometry, as for example [14, 27]. All these tools will be essential, in particular, to define dynamical models in the infinite-dimensional space of curves.

[2] We use the terms "motion" and "(shape) deformation" informally in this section, but in a way compatible with the definitions of [47]. In particular, "deformation" means a change in shape, and shape is defined as the quotient of closed planar curve with respect to a finite-dimensional group [30] (in this paper, the group is the identity).

2.1. Geometric Curves. We are interested in *geometric* curves, i.e., curves considered up to reparameterizations. Let $\mathrm{Diff}(\mathbb{S}^1)$ denote the group of diffeomorphisms of $\mathbb{S}^1$; given $\phi \in \mathrm{Diff}(\mathbb{S}^1)$ and a curve $c \in M$, the composition $c \circ \phi$ is a reparameterization of the c. For technical reasons, we identify the slightly more restrictive subspace M_f of all **freely immersed curves**, that are the curves $c \in M$ such that, if $\phi \in \mathrm{Diff}(S^1)$ and $c(\phi(\theta)) = c(\theta)$ for all θ, then ϕ is the identity. This space is a dense open subset of the space M; see [6] for a detailed proof. The advantage of this space is that we may define the space of **geometric curves** as the quotient space

$$B = M_f/\mathrm{Diff}(\mathbb{S}^1) \quad , \tag{2.2}$$

and it can be shown that B remains a manifold (see [35] or [6], Thm. 1.5; whereas the quotient $M/\mathrm{Diff}(\mathbb{S}^1)$ unfortunately is not a manifold). We will use the notation $[c]$ to indicate all possible parameterizations of the curve c; that is, $[c]$ is an element of B.

Assuming that the chosen Riemannian metric $\|h\|_c$ in M is reparameterization–invariant, then we can project it to B, so as to define a metric on B. The distance in B can be defined as follows.

Definition 2.1. *The **distance** $d : B \times B \to \mathbb{R}^+$ between two curves $[c_0] \in B$ and $[c_1] \in B$ is defined by*

$$d([c_0], [c_1]) = \inf_{\phi \in \mathit{Diff}(\mathbb{S}^1)} \inf_{\gamma \in \Gamma(c_0, c_1 \circ \phi)} \mathit{Len}(\gamma) \tag{2.3}$$

where

$$\Gamma(c_0, c_1) = \{\gamma : [0, 1] \to M_f : \gamma(0) = c_0, \gamma(1) = c_1\}$$

is the set of all smooth paths (of intermediate curves) connecting c_0 to c_1,

$$\mathit{Len}(\gamma) = \int_0^1 \|\dot\gamma(t)\|_{\gamma(t)}\, \mathrm{d}t, \tag{2.4}$$

is the length of a path γ, $\dot\gamma(t) \in T_{\gamma(t)} M_f$ is the velocity (that is, the time derivative) of $\gamma(t)$, and $\|\cdot\|_{\gamma(t)}$ is the norm on $T_{\gamma(t)} M_f$.

Definition 2.2. *A **minimal geodesic** in B between $[c_0]$ and $[c_1]$ is a path γ^* that attains the infimum in* (2.3)*. Equivalently, up to a time re-parameterization of the path γ^*, γ^* solves*

$$\inf_{\phi \in \mathit{Diff}(\mathbb{S}^1)} \inf_{\gamma \in \Gamma(c_0, c_1 \circ \phi)} \mathbb{E}(\gamma) \tag{2.5}$$

where

$$\mathbb{E}(\gamma) = \int_0^1 \|\dot\gamma(t)\|^2_{\gamma(t)}\, \mathrm{d}t \tag{2.6}$$

is the action of the path γ.

*A **critical geodesic** is a critical path for the action $\mathbb{E}$, that is, a solution to the associated Euler–Lagrange equations.*

Definition 2.3. *The **exponential map**, $\exp : TB \to B$, where TB is the tangent bundle of B, is*

$$\exp_{[c]}(h) = \gamma(1),$$

where $\gamma : [0, 1] \to B$ is the critical geodesic with $\dot\gamma(0) = h \in T_{[c]} B$.

3. A Geometric Sobolev-Type Metric. In this section, we define a Riemannian metric on the space of curves M; this metric is invariant with respect to reparameterizations of the curve. This metric will allow us to compute geodesics in B, distances between contours, gradients for active contours, etc.

For any fixed immersed curve c, let $L(c)$ be the length of c, and given any $g : \mathbb{S}^1 \to \mathbb{R}^2$, let

$$D_s g \doteq \frac{g'}{|c'|}$$

be the derivative with respect to (w.r.t.) arclength, and

$$\int_c g(s)\,\mathrm{d}s \doteq \int_{\mathbb{S}^1} g(\theta)|c'(\theta)|\,\mathrm{d}\theta$$
$$\fint_c g(s)\,\mathrm{d}s \doteq \frac{1}{L(c)} \int_c g(s)\,\mathrm{d}s$$

denote the integral and the mean with respect to arclength. We will often use the notation

$$\overline{g} = \fint_c g(s)\,\mathrm{d}s$$

(not to be confused with the complex conjugate, which we will denote by g^*); we will call $\overline{c}$ the *centroid* of c.

In the active contour literature, one defines an energy functional $E_{ac} : B \to \mathbb{R}$ that is constructed so that the minimal energy contour $[c] \in B$ represents the boundary of an object of interest in an image. Typically, a gradient descent procedure is used to optimize E_{ac}. To define a gradient, one needs a Riemannian metric, that is often tacitly assumed to be

$$\langle h, k \rangle_{H^0} \doteq \fint_c h(s) \cdot k(s)\,\mathrm{d}s, \tag{3.1}$$

where s is the arclength parameter of c.[3] (We omit the dependency of the metric on c, for ease of notation.) However, it is shown in [33] that in this metric, the distance between any two curves in B is zero. Therefore, in [49] we considered the following geometric Sobolev-type metric

$$\langle h, k \rangle_{\tilde{H}^1} \doteq \overline{h} \cdot \overline{k} + \lambda L(c) \int_c D_s h \cdot D_s k\,\mathrm{d}s, \tag{3.2}$$

where $\lambda > 0$ is a (constant) weight.[4] This metric $\tilde{H}^1$ was shown to yield favorable properties for active contours (i.e., gradient descent of E_{ac}) [51, 50, 52]. Moreover this metric defines a well-behaved Riemannian geometry, in that the distance between

[3]Note that in this section we are considering "geometric metrics" of curves, where the derivations and integrals are performed w.r.t. the arc parameter; these metrics are distinguished by using the letter "H", in different forms. Later on we will instead use the notation $\mathbb{L}^2$ for the standard Hilbert metric where integration is performed in the parametric variable, as usual.

[4]More classical Sobolev–type metrics for active contours were also presented in [10, 9, 51, 52]. An overview of Sobolev–type metrics, methods, and mathematical result was presented in [35]; in Section 4.3 of [35] it is shown that, for a large class of Sobolev metrics, critical geodesics exist for short time and smooth initial data.

different curves is positive. However, while having some of the appropriate properties for our applications, it is not particularly easy to compute geodesics in this metric. Moreover, the shape space obtained by coupling the immersed curves with this metric is not decomposable into components that are natural for visual tracking applications in computer vision. Therefore, we propose in the remainder of this paper a new variant which was constructed deliberately for its favorable properties in such applications.

3.1. A New Sobolev–Type Metric. We recall that the Gâteaux derivative of a function $f : M \to \mathbb{R}^k$ is defined by

$$Df(c;h) \doteq \frac{d}{dt} f(c+th)\bigg|_{t=0} = \lim_{t\to 0} \frac{f(c+th)-f(c)}{t} \quad .$$

The Gâteaux derivatives of the centroid and of the length

$$D(\overline{c})(c;h) = \fint_c p(h)\,\mathrm{d}s$$
$$DL(c)(c;h) = -\int_c h \cdot D_s^2 c\,\mathrm{d}s$$

where

$$p(h) \doteq h - (h \cdot D_s c) D_s c - (h \cdot D_s^2 c)(c - \overline{c}) \quad .$$

To define the new metric $\mathbb{H}$, we first define the following decomposition for $c \in M$ and $h \in T_c M$:

$$h = h^t + h^l (c - \overline{c}) + L(c) h^d \tag{3.3}$$

where h^t is the component of h that changes the centroid of c, $h^l(c-\overline{c})$ is the component of h that changes the scale (length) of c, and h^d is the component of h that deforms c. The components h^t and h^l of h are defined as

$$h^t = D(\overline{c})(c;h) = \fint_c p(h)\,\mathrm{d}s \in \mathbb{R}^2 \tag{3.4}$$

$$h^l = D(\log L(c))(c;h) = -\fint_c h \cdot D_s^2 c\,\mathrm{d}s \in \mathbb{R} \ . \tag{3.5}$$

$$h^d = \frac{1}{L(c)} [h - h^t - h^l (c - \overline{c})] \tag{3.6}$$

The component h^d deforms the curve without scaling or translating, since

$$D(L(c))(c;h^d) = 0 \quad , \quad D\overline{c}(c;h^d) = 0 \quad .$$

Definition 3.1. *If $h, k \in T_c M$ are decomposed as above, then we define the Riemannian metric $\mathbb{H}$ as*

$$\langle h, k \rangle_{\mathbb{H}} \doteq h^t \cdot k^t + \lambda_l h^l k^l + \lambda_d L(c)^2 \fint_c D_s h^d \cdot D_s k^d \,\mathrm{d}s, \tag{3.7}$$

where the first two products are the Euclidean dot products, the last term is a normalized geometric Sobolev metric, and $\lambda_l, \lambda_d > 0$ are (constant) weights.

Note that in the notation $\langle h, k \rangle_{\mathbb{H}}$, we have omitted the dependency of the scalar product on c, for ease of notation. Note also that the third term of the metric may be rewritten directly as a function of $h \in T_cM$ by using the identity

$$L(c)^2 \fint_c D_s h^d \cdot D_s k^d \,\mathrm{d}s = \fint_c D_s h \cdot D_s k \,\mathrm{d}s - \fint_c D_s h \cdot D_s c \,\mathrm{d}s \fint_c D_s c \cdot D_s k \,\mathrm{d}s \ . \quad (3.8)$$

This new metric enjoys the following properties:

1. Centroid translations, scale changes and deformations of the curve are orthogonal. Moreover, the space of curves can be decomposed into a product space consisting of three components as shown in Thm. 3.4 below.
2. Sobolev-type metrics favor *smooth* but otherwise unrestricted infinite-dimensional deformations [51] and they have a coarse-to-fine evolution behavior [52]. For this reason, the old metric $\tilde{H}^1$ has proven useful in frame-wise object detection/image segmentation for visual tracking.
   The new metric $\mathbb{H}$ is metrically equivalent to the old metric $\tilde{H}^1$, indeed
   THEOREM 3.2.
   $$a_1 \frac{L(c)}{1+L(c)} \ \|h\|_{\mathbb{H}} \le \|h\|_{\tilde{H}^1} \le a_2(1+L(c)) \ \|h\|_{\mathbb{H}}$$
   where $0 < a_1 < a_2$ *are constants depending on* $\lambda, \lambda_l, \lambda_d$. (The proof is in appendix A.1.)
   Therefore the new metric $\mathbb{H}$ inherits the favorable properties of the old metric $\tilde{H}^1$ for shape optimization tasks.
3. As was the case for the old metric $\tilde{H}^1$, there is a fast and easy way to compute gradients of commonly used energies with respect to the new metric $\mathbb{H}$. The method will be presented in Prop. 4.6.
4. Geodesics in this new metric (i.e., the optimization problem in (2.3)) can be numerically computed efficiently. The method is explained in next section.

For all these reasons, this new metric seems a state of the art choice for addressing problems in Shape Theory, when the shape of interest can be represented as a curve: indeed, it entails a sound mathematical model that can address problems in shape analysis and shape optimization, and any desired combination of the two.

3.2. Space Decomposition. We will find it useful to define a submanifold M_d of M:

DEFINITION 3.3. *Let*

$$M_d = \{c \in M : L(c) = 1, \overline{c} = 0\} \quad , \quad (3.9)$$

that is the space of all smooth immersed curves with unit length and with centroid at the origin. This is a smooth submanifold of M (the proof follows from a corollary of Nash–Moser theorem, see [19]). Its tangent space at $\tilde{c} \in M$ is

$$T_{\tilde{c}} M_d = \left\{ h \in T_{\tilde{c}} M \ \mid \ \int_{\tilde{c}} (D_s^2 \tilde{c}) \cdot h \,\mathrm{d}s = 0, \int_{\tilde{c}} p(h) \,\mathrm{d}s = 0 \right\} \ . \quad (3.10)$$

We associate the Euclidean metric to $\mathbb{R}^n \times \mathbb{R}$ and the metric

$$\langle h, k \rangle_{M_d} = \int_{\tilde{c}} D_s h \cdot D_s k \ \ \mathrm{d}s \quad (3.11)$$

to M_d. This metric is the restriction of the metric $\mathbb{H}$ to M_d. The metric $\mathbb{H}$ is associated to an isometry between the space of curves M and the space $\mathbb{R}^2 \times \mathbb{R} \times M_d$.

THEOREM 3.4. *Let $\lambda_l = \lambda_d = 1$ (in (3.1)) for simplicity. We define a map and its inverse*

$$c \in M \mapsto \left(v = \overline{c}\ ,\ l = \log L(c)\ ,\ \tilde{c} = \frac{c - \overline{c}}{L(c)} \right) \in \mathbb{R}^2 \times \mathbb{R} \times M_d, \tag{3.12}$$

$$(v, l, \tilde{c}) \in \mathbb{R}^2 \times \mathbb{R} \times M_d \mapsto v + e^l \tilde{c} \in M. \tag{3.13}$$

This map is an isometry. (The proof is in appendix A.2).

To the best of our knowledge, the metric $\mathbb{H}$ is the first example of a Sobolev–type metric of immersed curves to exhibit this useful decomposition of the entire space M. Other known metrics would provide a decomposition only of the infinitesimal motions h, *i.e.*, a decomposition of the tangent space $T_c M$ rather than the space M itself. This decomposition moreover greatly simplifies the proof of some of the mathematical results in the following sections.

3.3. Computing Geodesics and the Exponential Map. Let

$$C : \mathbb{S}^1 \times [0,1] \to \mathbb{R}^2,\ (\theta, t) \mapsto C(\theta, t)$$

denote a time varying family of closed curves (i.e., a homotopy) corresponding to a path $\gamma : [0,1] \to M$, i.e., $C(\theta,t) = \gamma(t)(\theta)$. We will write either $\partial_t C$ or $\dot{C}$ to denote the time derivative of C. We have that

$$\|\partial_t C\|_{\mathbb{H}}^2 = |\partial_t \overline{C}|^2 + \lambda_l (\partial_t (\log L(C)))^2 + \lambda_d L(c)^2 \fint_C |D_s (\partial_t C)^d|^2\, \mathrm{d}s \quad . \tag{3.14}$$

Following (2.6), let

$$\mathbb{E}(C) \doteq \int_0^1 \|\partial_t C\|_{\mathbb{H}}^2\, \mathrm{d}t$$

be the *action* of the homotopy C. Using the above fact and some manipulations, one can show that geodesics in this metric are invariant to scale and translations.

PROPOSITION 3.5 (Invariance of the action $\mathbb{E}$). *Let $c_0, c_1 \in M$ and let*

$$\tilde{c}_1 = v + e^{\rho}(c_1 - \overline{c_1}) + \overline{c_1}$$

be a scaling and translation of c_1. Suppose that C is a homotopy connecting c_0 to c_1, and let

$$\tilde{C} = tv + e^{t\rho}(C - \overline{C}) + \overline{C}$$

be a homotopy connecting c_0 to $\tilde{c}_1$; then

$$\mathbb{E}(\tilde{C}) = \mathbb{E}(C) + const$$

where the "constant term" depends only on the end curves c_0, c_1 and v, ρ. As a corollary, C is a geodesic connecting c_0 to c_1 if and only if $\tilde{C}$ is a geodesic connecting c_0 to $\tilde{c}_1$. This result can be seen as a corollary of Thm. 3.4.

The above is also related to the following conservation laws:

PROPOSITION 3.6 (Momenta). *Suppose that C is a geodesic, then the following quantities are conserved:*

- [translation] $\partial_t \overline{C}$ *is constant;*

- [scaling] $\partial_t(\log L(C))$ *is constant;*
- [rotation] *the angular momentum (that may be expressed in two equal ways)*

$$\fint_C (AD_sC)\cdot(\partial_t D_sC)\,\mathrm{d}s = \fint_C (AD_sC)\cdot(D_s\partial_t C)\,\mathrm{d}s \tag{3.15}$$

  is constant, for any antisymmetric matrix A;
- [reparametrization] $(D_sC)\cdot(D_s^2\partial_t C)$ *is constant in t, for any fixed* $\theta \in \mathbb{S}^1$.

(The proof is in Appendix A.3.)

This, in particular, means that, along a geodesic C connecting c_0 to c_1,

$$\overline{C} = (1-t)\overline{c_0} + t\overline{c_1} \tag{3.16}$$

$$\log L(C) = (1-t)\log L(c_0) + t\log L(c_1). \tag{3.17}$$

The previous results imply that to compute a minimal geodesic in M between c_0 and c_1, we apply the following procedure:

1. define

$$\tilde{c}_0 \doteq \frac{c_0 - \overline{c_0}}{L(c_0)} \quad , \quad \tilde{c}_1 \doteq \frac{c_1 - \overline{c_1}}{L(c_1)} \quad ;$$

2. compute a geodesic $\tilde{C}$ between $\tilde{c}_0$ and $\tilde{c}_1$ in the space M_d
3. rebuild the geodesic in M

$$C(t,\cdot) = L^{1-t}(c_0)L^t(c_1)\tilde{C}(t,\cdot) + (1-t)\overline{c_0} + t\overline{c_1} \quad .$$

3.3.1. Representing Smooth Curves Using the Square Root Lifting. We have therefore reduced the problem of computing geodesics in M to computing geodesics in the space M_d of unit length curves with centroid at the origin. To this end, we will identify the plane $\mathbb{R}^2$ with the complex numbers $\mathbb{C}$, and consider curves as smooth maps $c : \mathbb{R} \to \mathbb{C}$ that are periodic of period 1.

Given two smooth functions $e, f : \mathbb{R} \to \mathbb{R}$ we define the map Φ introduced by Younes et al. in [60, 61] by

$$c(\theta) = \Phi(e,f)(\theta) \doteq c(0) + \frac{1}{2}\int_0^\theta (e+if)^2(\xi)\,\mathrm{d}\xi \tag{3.18}$$

where i denotes the imaginary unit; this map uniquely identifies a curve up to the choice of the base point $c(0)$, or equivalently, up to the choice of the centroid $\overline{c}$.

Note that for $c = \Phi(e,f)$ to be a closed curve we must have that

$$0 = c(1) - c(0) = \frac{1}{2}\int_0^1 (e+if)^2(\theta)\,\mathrm{d}\theta = \frac{1}{2}\int_0^1 [e^2(\theta) - f^2(\theta) + 2ie(\theta)f(\theta)]\,\mathrm{d}\theta, \tag{3.19}$$

and for the curve to be of unit length we must have that

$$1 = \int_0^1 |\dot{c}(\theta)|\,\mathrm{d}\theta = \frac{1}{2}\int_0^1 (e^2(\theta) + f^2(\theta))\,\mathrm{d}\theta. \tag{3.20}$$

The conditions (3.19) and (3.20) imply that the pair (e,f) belongs to

$$\mathbf{St}(2, C^\infty) = \left\{(e,f) \in C^\infty \times C^\infty \;\middle|\; \|e\|_{\mathbb{L}^2} = \|f\|_{\mathbb{L}^2} = 1,\, \langle e,f\rangle_{\mathbb{L}^2} = 0\right\} \tag{3.21}$$

where the above $\mathbb{L}^2$ norms and inner product are the standard ones on $\mathbb{L}^2([0,1])$. $\mathbf{St}(2,C^\infty)$ is known as a *Stiefel* manifold. It is a Riemannian manifold when we use the metric induced from the scalar product $\mathbb{L}^2\times\mathbb{L}^2$ on the frames (e,f).

Vice versa, let c be a closed unit length immersed smooth curve. We express c' in polar coordinates as

$$c'(\theta)=r(\theta)(\cos\varphi(\theta)+i\sin\varphi(\theta)) \quad .$$

We can then define an inverse of Φ (called the *square-root lifting*) by setting

$$e(\theta)+if(\theta)=\Phi^{-1}(c)(\theta)=\sqrt{2r(\theta)}(\cos\frac{\varphi(\theta)}{2}+i\sin\frac{\varphi(\theta)}{2}), \tag{3.22}$$

Note that (e,f) and $(-e,-f)$ are the only two inverses of c.

We identify inside $\mathbf{St}(2,C^\infty)$ an open subset $\mathbf{St}^0$ of all smooth frames (e,f) that represent the curves $c\in M_d$: then $\Phi:\mathbf{St}^0\to M_d$ is a smooth two-fold covering. It is shown in [61] that Φ is a Riemannian isometry from $\mathbf{St}^0$ to M_d endowed with a Sobolev–type metric.

THEOREM 3.7 (Theorem 2.2 in [61]). *Let $\tilde c\in M_d$, and $h\in T_{\tilde c}M_d$ (see (3.10)) and $(e,f)\in\mathbf{St}^0$, $(\delta e,\delta f)\in T_{(e,f)}\mathbf{St}^0$ be the corresponding Stiefel representations, i.e.,*

$$D\Phi(e,f;\delta e,\delta f)=h \ .$$

Then

$$\int_{\tilde c}|D_s h|^2\,\mathrm{d}s=2\int_0^1(\delta e)^2+(\delta f)^2\,\mathrm{d}\theta \quad .$$

To exploit this theorem, we associate to M_d the (restriction of) the Sobolev–type metric $\int_{\tilde c}|D_s h|^2\,\mathrm{d}s$; then Φ maps isometrically the (restriction of) the metric $\mathbb{L}^2\times\mathbb{L}^2$ in $\mathbf{St}^0$ to the chosen metric on M_d. So this result couples perfectly with the isometry shown in Thm. 3.4 before.

3.3.2. Completing $\mathbf{St}(2,C^\infty)$ to $\mathbf{St}(2,\mathbb{L}^2)$. The space $\mathbf{St}(2,C^\infty)$ is not a complete smooth Riemannian manifold; its metric completion is the space $\mathbf{St}(2,\mathbb{L}^2)$ of all orthonormal frames (e,f) of two generic vectors $e,f\in\mathbb{L}^2=\mathbb{L}^2([0,1])$. $\mathbf{St}(2,\mathbb{L}^2)$ has many interesting properties:

- $\mathbf{St}(2,\mathbb{L}^2)$ is a smooth embedded submanifold of $\mathbb{L}^2\times\mathbb{L}^2$.
- $\mathbf{St}(2,\mathbb{L}^2)$ is a complete smooth Riemannian manifold modeled on a Hilbert space. This implies that the exponential map is well defined. We will show in the next section that the exponential map can be written in closed form and computed efficiently. (The formula proves that any two given pairs (e_0,f_0) and (e_1,f_1) can be connected by a critical geodesic; that is, the exponential map is surjective).
- Completeness is also an important hypothesis in any mathematical proof that would aim to prove that an optimization method is well posed.
- A frame $(e,f)\in\mathbf{St}(2,\mathbb{L}^2)$ can be mapped to a closed (possibly non-smooth) curve using the map Φ; but the map is not a two-fold covering, that is, a curve has many representations in $\mathbf{St}(2,\mathbb{L}^2)$.
- Vice–versa, any closed curve c that is absolutely continuous (that is, c' exists as an integrable function) can be represented by a pair $(e,f)\in\mathbf{St}(2,\mathbb{L}^2)$.

For these reasons, we will consider $\mathbf{St}(2,\mathbb{L}^2)$ instead of $\mathbf{St}(2,C^\infty)$ in the rest of the paper.

3.3.3. Computing Critical Geodesics. Due to the above theorems and remarks, we now present the calculus of geodesics in $\mathbf{St}(2, \mathbb{L}^2)$.

Classically, the Stiefel manifold $\mathbf{St}(p, \mathbb{R}^n)$ is defined as the set of all frames composed of p orthonormal vectors in $\mathbb{R}^n$ (with $1 \leq p \leq n$); those frames are represented as $n \times p$ matrices. Geodesics in Stiefel manifolds $\mathbf{St}(p, \mathbb{R}^n)$ are known to have closed form solutions as demonstrated by Edelman et al. [15].[5]

PROPOSITION 3.8 (Exponential Map in $\mathbf{St}(p, \mathbb{R}^n)$). *Let $Y : [0,1] \to \mathbf{St}(p, \mathbb{R}^n)$ be a path, suppose that $\mathbf{St}(p, \mathbb{R}^n)$ is endowed with the Euclidean metric, i.e.,*

$$\langle A, B \rangle = tr(A^T B) \quad ,$$

then the geodesic equation is

$$\ddot{Y} + Y(\dot{Y}^T \dot{Y}) = 0 \quad . \tag{3.23}$$

The solution is

$$(Y(t)e^{At}, \dot{Y}(t)e^{At}) = (Y(0), \dot{Y}(0)) \exp t \begin{pmatrix} A & -S \\ Id & A \end{pmatrix} \tag{3.24}$$

where $A = Y^T(0)\dot{Y}(0)$, $S = \dot{Y}^T(0)\dot{Y}(0)$, and Id is the $p \times p$ identity matrix. The proof and discussion of these results is in Section 2.2.2 in [15].

The solution in (3.24), while written for $\mathbf{St}(p, \mathbb{R}^n)$, extends to $\mathbf{St}(2, \mathbb{L}^2)$. Indeed, (3.24) shows that the columns of $Y(t), \dot{Y}(t)$ remain in the space spanned by the columns of $Y(0), \dot{Y}(0)$ for all t.

PROPOSITION 3.9 (Exponential Map in $\mathbf{St}(2, \mathbb{L}^2)$). *Let $(e, f) : [0,1] \to \mathbf{St}(2, \mathbb{L}^2)$ be a geodesic path such that*

$$(e(0), f(0)) = (e^*, f^*) \in \mathbf{St}(2, \mathbb{L}^2) \quad ,$$

and

$$(\dot{e}(0), \dot{f}(0)) = (\delta e, \delta f) \in T_{(e^*, f^*)}\mathbf{St}(2, \mathbb{L}^2) \; .$$

Define an orthonormal set[6]

$$\mathcal{B} = \{e^*, f^*, \tilde{e}, \tilde{f}\} \subset span(\{e^*, f^*, \delta e, \delta f\}) \tag{3.25}$$

according to the usual $\mathbb{L}^2$ metric. Then the geodesic in $\mathbf{St}(2, \mathbb{L}^2)$ is given by

$$e(t) = Y_1^1(t)e^* + Y_1^2(t)f^* + Y_1^3(t)\tilde{e} + Y_1^4(t)\tilde{f}$$
$$f(t) = Y_2^1(t)e^* + Y_2^2(t)f^* + Y_2^3(t)\tilde{e} + Y_2^4(t)\tilde{f}$$

where Y_j^i denotes the i^{th} component of $Y_j \in \mathbb{R}^4$, $Y : [0,1] \to \mathbf{St}(2, \mathbb{R}^4)$ is the geodesic in $\mathbf{St}(2, \mathbb{R}^4)$ that satisfies

$$Y(0) = ((1,0,0,0)^T, (0,1,0,0)^T) \tag{3.26}$$
$$\dot{Y}(0) = (a, b) \in T_{Y(0)}\mathbf{St}(2, \mathbb{R}^4), \tag{3.27}$$

and (a, b) are the representations of $\delta e, \delta f$ relative to $\mathcal{B}$. The geodesic $\gamma : [0,1] \to M_d$ can then be recovered from the geodesic in $\mathbf{St}(2, \mathbb{L}^2)$ via the isometry Φ; but note that, even if the initial curve is smooth and immersed and vector field is smooth, it is not guaranteed that the curve will be immersed for all t (cf. Sec. 3.3.2, and the examples in [61]).

[5] [15] credits a personal communication by R. A. Lippert for the final closed form formula (3.24).
[6] If $\{e^*, f^*, \delta e, \delta f\}$ do not span a 4 dimensional space, then $\tilde{f}$ may be chosen arbitrarily.

3.3.4. Computing Minimal Geodesics. The formula (3.24) gives the geodesic as a function of the initial position and direction; this is the exponential map. However, to compute geodesics between two curves (the so called *logarithmic map*), it is necessary to have a formula for Y in terms of the boundary conditions $Y(0)$ and $Y(1)$. We are not aware of such an explicit formula and, therefore, we use an iterative algorithm that computes the initial direction $\dot{Y}(0)$ of the geodesic Y such that $Y(0) = Y_0$ and $Y(1) = Y_1$.

As in the previous proposition, we can reduce the computation to $\mathbf{St}(2, \mathbb{R}^4)$: indeed we represent the end curves as two frames (e_0, f_0) and (e_1, f_1) respectively, and then define an orthonormal set

$$\mathcal{B} = \{e_0, f_0, \tilde{e}, \tilde{f}\} \subset \operatorname{span}(\{e_0, f_0, e_1, f_1\}).$$

In this coordinate system, the end curves are represented as $Y_0, Y_1 \in \mathbb{R}^{4\times 2}$, and Y_0 is given by (3.26). All possible tangent vectors at Y_0 are

$$\dot{Y}(0) = ((0, \alpha, v_1, v_3)^T, (-\alpha, 0, v_2, v_4)^T))$$

with $\alpha, v_1, v_2, v_3, v_4 \in \mathbb{R}$, in conformity with the representation in eqn. (2.6) in [15].

To compute the geodesic, we minimize the energy $E : \mathbb{R}^5 \to \mathbb{R}^+$,

$$E(\alpha, v_1, v_2, v_3, v_4) = |Y(1) - Y_1|^2 \tag{3.28}$$

where $Y(1)$ is given according to (3.24),

$$\begin{aligned} Y(1) &= (Y(0), \dot{Y}(0)) \exp \begin{pmatrix} A & -S \\ \mathrm{Id}_{2\times 2} & A \end{pmatrix} \mathrm{Id}_{4\times 2} e^{-A} \\ A &= \begin{pmatrix} 0 & -\alpha \\ \alpha & 0 \end{pmatrix}, \quad S = \begin{pmatrix} \alpha^2 + v_1^2 + v_3^2 & v_1 v_2 + v_3 v_4 \\ v_1 v_2 + v_3 v_4 & \alpha^2 + v_2^2 + v_4^2 \end{pmatrix}, \end{aligned}$$

where $\mathrm{Id}_{4\times 2} = ((1, 0, 0, 0)^T, (0, 1, 0, 0)^T)$. Note the energy E is not convex.

We minimize (3.28) by standard gradient descent in $\mathbb{R}^5$, initializing the descent with $(\alpha, v_1, v_2, v_3, v_4) = (0, 0, 0, 0, 0)$. The gradient is computed as follows:

Proposition 3.10. *The partial derivatives of the energy E in* (3.28) *are given by*

$$\begin{aligned} \partial_* E(\alpha, v_1, v_2, v_3, v_4) = (Y(1) - Y_1) \cdot \Big[&(0_{4\times 2}, \partial_* \dot{Y}(0)) \exp(N)\, Id_{4\times 2}\, e^{-A} \\ &+ (Y(0), \dot{Y}(0)) \int_0^1 \exp(tN) \partial_* N \exp((1-t)N)\, \mathrm{d}t\, Id_{4\times 2} e^{-A} \\ &+ (Y(0), \dot{Y}(0)) \exp(N)\, Id_{4\times 2}\, e^{-A} \partial_* A \Big] \end{aligned} \tag{3.29}$$

where $* = \alpha, v_1, v_2, v_3, v_4$,

$$N = \begin{pmatrix} A & -S \\ Id_{2\times 2} & A \end{pmatrix},$$

the partials of A are

$$\partial_\alpha A = \begin{pmatrix} 0 & -1 \\ 1 & 0 \end{pmatrix}, \text{ and } \partial_{v_i} A = 0_{2\times 2} \text{ for } i = 1, 2, 3, 4,$$

and the partials of S are

$$\partial_\alpha S = 2\alpha Id_{2\times 2}, \partial_{v_1} S = \begin{pmatrix} 2v_1 & v_2 \\ v_2 & 0 \end{pmatrix}, \partial_{v_2} S = \begin{pmatrix} 0 & v_1 \\ v_1 & 2v_2 \end{pmatrix},$$
$$\partial_{v_3} S = \begin{pmatrix} 2v_3 & v_4 \\ v_4 & 0 \end{pmatrix}, \partial_{v_3} S = \begin{pmatrix} 0 & v_3 \\ v_3 & 2v_4 \end{pmatrix}$$

Proof. This is a standard calculation based on the matrix differentiation formula

$$D(\exp X)(X; Z) = \int_0^1 \exp(tX) Z \exp((1-t)X)\, \mathrm{d}t,$$

which can be found in [31].[7] Note that when X and Z commute, then $D(\exp X)(X; Z) = \exp(X)Z$. □ The derivative of the matrix exponential can be computed efficiently using a technique resembling the Fast Fourier Transform (see Appendix B for details). The geodesic connecting Y_0 to Y_1 is then obtained by setting $Y(0) = Y_0$ and $\dot{Y}(0) = ((0, \alpha^*, v_1^*, v_3^*)^T, (-\alpha^*, 0, v_2^*, v_4^*)^T)$ where $(\alpha^*, v_1^*, v_2^*, v_3^*, v_4^*)$ is the minimum point of (3.28).

3.4. Geodesics in the Space of Geometric Curves, B**.** Up to this point, we have specified how to compute geodesics, and the exponential map in M according to the metric $\mathbb{H}$; however, we are interested in these operations in the geometric space B. To be mathematically precise, in this section we will consider M to be the space of all freely immersed smooth curves.

We first define two objects of interest. We define the *vertical space* as

$$V_c M = \{h \in T_c M : h = \beta c',\ \beta : \mathbb{S}^1 \to \mathbb{R}\}. \tag{3.30}$$

This is the set of infinitesimal deformations of c that do not change the geometry of the curve c, but only its parameterization. We then define the *horizontal space* as

$$W_c M \doteq (V_c M)^\perp = \{h \in T_c M : \langle h, k\rangle_{\mathbb{H}} = 0,\ \forall k \in V_c M\}. \tag{3.31}$$

We use the horizontal space $W_c M$ as a model of the tangent space $T_{[c]}B$.

Geodesics in B (with the metric induced from M) correspond to geodesics in M provided they are horizontal, i.e., $\dot\gamma(t) \in W_{\gamma(t)} M$, $\forall t$. Equivalently, it is enough that $\dot\gamma(1) \in W_{\gamma(1)} M$ and γ be a geodesic in M for γ to be a geodesic in B. We now give the condition to determine whether $\dot\gamma(1) \in W_{\gamma(1)} M$, which can be found in [61]. As a first step we consider $\phi \in \mathrm{Diff}(\mathbb{S}^1)$ such that $\phi(0) = 0$: then, by direct computation,

$$\Phi(e, f)(\phi^{-1}(\theta)) = c(0) + \frac{1}{2}\int_0^{\phi^{-1}(\theta)} (e + if)^2(\xi)\, \mathrm{d}\xi =$$
$$c(0) + \frac{1}{2}\int_0^{\theta} (e + if)^2(\phi(\xi))\phi'(\xi)\, \mathrm{d}\xi = \Phi\left(\sqrt{\phi'}\,(e\circ\phi), \sqrt{\phi'}\,(f\circ\phi)\right)(\theta)$$

where $\phi' = \mathrm{d}\phi/\mathrm{d}\theta$ is the derivative of ϕ. Therefore, the action of reparameterization on a point $(e, f) \in \mathbf{St}(2, C^\infty)$ is

$$(e, f) \mapsto \sqrt{\phi'}\,(e\circ\phi, f\circ\phi),$$

[7] A more general result for infinite dimensional Lie manifolds has been proven in [18].

and the differential of the action above evaluated at the identity in the direction $\beta : \mathbb{S}^1 \to \mathbb{R}$ is

$$\left(\frac{1}{2}\beta' e + \beta e', \frac{1}{2}\beta' f + \beta f'\right) \quad .$$

The collection of all such differentials above for all β is the vertical space at (e, f). For $(\delta e, \delta f) \in T_{(e,f)}\mathbf{St}(2, C^\infty)$ to be in the horizontal space, it must be orthogonal to all vertical perturbations:

$$\left\langle \delta e, \frac{1}{2}\beta' e + \beta e' \right\rangle_{\mathbb{L}^2} + \left\langle \delta f, \frac{1}{2}\beta' f + \beta f' \right\rangle_{\mathbb{L}^2} = \\ \frac{1}{2}\left\langle \beta, e'\delta e - e(\delta e)' \right\rangle_{\mathbb{L}^2} + \frac{1}{2}\left\langle \beta, f'\delta f - f(\delta f)' \right\rangle_{\mathbb{L}^2} = 0,$$

for all β, that is

$$\Omega(e, \delta e) + \Omega(f, \delta f) = 0 \tag{3.32}$$

where

$$\Omega(a, b) \doteq ab' - ba'. \tag{3.33}$$

To compute a geodesic between $[c_0], [c_1] \in B$, we use the algorithm below.

Algorithm 3.11 (Computing Geodesics in $\mathbf{St}(2, C^\infty)/\mathrm{Diff}(\mathbb{S}^1)$). *Let $\phi_0 \in Diff(\mathbb{S}^1)$ be an initial reparameterization of the end curve c_1 in its Stiefel representation (one possible initialization is given below in Remark 3.12). Define a sequence $\phi_k \in Diff(\mathbb{S}^1)$ iterating the following steps*

1. *Compute the geodesic, $(e_{\phi_k}(t), f_{\phi_k}(t))$, $t \in [0, 1]$, in $\mathbf{St}(2, C^\infty)$ between (e_0, f_0) and $\sqrt{\dot{\phi}_k}(e_1 \circ \phi_k, f_1 \circ \phi_k)$.*
2. *Compute a $\beta : \mathbb{S}^1 \to \mathbb{R}$ so that, defining*

$$(v_e, v_f) = (\frac{1}{2}\beta' e_{\phi_k}(1) + \beta e'_{\phi_k}(1), \frac{1}{2}\beta' f_{\phi_k}(1) + \beta f'_{\phi_k}(1)) \tag{3.34}$$

we have that $(e'_{\phi_k}(1) - v_e, f'_{\phi_k}(1) - v_f)$ is horizontal; this β must solve

$$\Omega(e_{\phi_k}(1), e'_{\phi_k}(1) - v_e) + \Omega(f_{\phi_k}(1), f'_{\phi_k}(1) - v_f) = 0$$

that is

$$\Omega(e_{\phi_k}(1), v_e) + \Omega(f_{\phi_k}(1), v_f) = \Omega(e_{\phi_k}(1), e'_{\phi_k}(1)) + \Omega(f_{\phi_k}(1), f'_{\phi_k}(1)) \quad . \tag{3.35}$$

Note that (3.35) *simplifies to*

$$\frac{1}{2}\beta''(e^2 + f^2) + \beta'(ee' + ff') - \beta\Big((e')^2 - ee'' + (f')^2 - ff''\Big) = \Omega(e, \dot{e}) + \Omega(f, \dot{f}) \tag{3.36}$$

where we have used a simplified notation $e = e_{\phi_k}(1)$, $f = f_{\phi_k}(1)$, $\dot{e} = \dot{e}_{\phi_k}(1)$, and $\dot{f} = \dot{f}_{\phi_k}(1)$. Note that the discretization of (3.36) *is given in Appendix D.*
3. *Set $\phi_{k+1} = \phi_k - \varepsilon\beta$ where $\varepsilon > 0$ is small.*

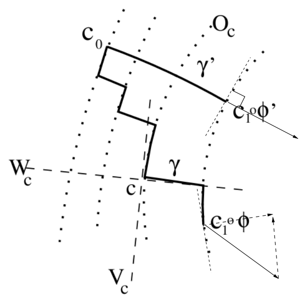

FIG. 3.1. The dashed lines represent equivalence classes of curves (O_c is the orbit $[c]$), and W_c is the horizontal space to c. To compute geodesics in B, we compute the geodesic in M between c_0 and $c_1 \circ \phi$ (the staircase path), project $\dot{\gamma}$ to its vertical component (tangent to $O_{c_1 \circ \phi}$), and move c_1 to another representative determined by the vertical component, and iterate the process until the vertical component becomes zero.

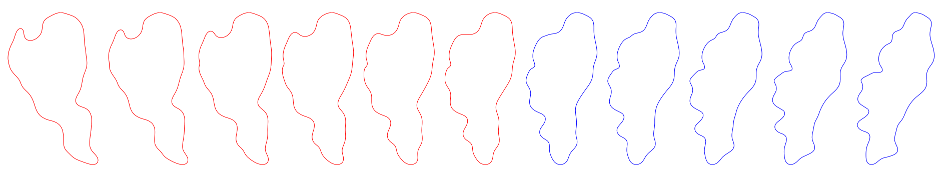

FIG. 3.2. *Example illustration of a geodesic in B. The geodesic is computed between the first (left-most) and the last red curve (time $t = 0$ and $t = 1$), and intermediate curves (interpolation) are shown in between. The blue curves ($t = 1$ to $t = 2$) are the continuation of the geodesic (extrapolation) from the last red curve. It can be seen that the extrapolation does not simply change the pose of the contour, but also alters its shape (i.e., it "deforms").*

Figure 3.1 illustrates this process.

REMARK 3.12. *The above algorithm is not guaranteed to converge to the global optimum reparameterization ϕ^* of the geodesic distance in $\mathbf{St}(2, C^\infty)$. In order to help avoid convergence to a local minimum, we perform a direct search for the optimal base point rotation $\phi_0(\theta) = \theta + a$, where $a \in \mathbb{S}^1$ before iterating the above steps.* The geodesic $(e_{\phi_k}(t), f_{\phi_k}(t))$, $t \in [0, 1]$ (in $\mathbf{St}(2, C^\infty)$) for large k will approximate the geodesic in $\mathbf{St}(2, C^\infty)/\mathrm{Diff}(\mathbb{S}^1)$, and hence $\Phi(e_{\phi_k}(t), f_{\phi_k}(t))$, $t \in [0, 1]$ approximates the geodesic in B.

Figure 3.2 shows an example geodesic in B.

3.5. Parallel Transport. In the next section we will discuss a dynamical model for tracking deforming shapes. To this end, we recall this definition, that is standard in Riemannian Geometry.

DEFINITION 3.13. *Suppose that M is a Riemannian manifold. Given a path $\gamma : [a, b] \to M$, the* parallel transport

$$P_\gamma : T_{\gamma(a)}M \to T_{\gamma(b)}M$$

along γ of the tangent vector $h \in T_{\gamma(a)}M$ is defined as

$$P_\gamma(h) = V(b)$$

where the vector field $V(t) \in T_{\gamma(t)}M$ is such that

$$\begin{cases} \nabla_{\dot{\gamma}(t)} V(t) = 0 \quad \forall t \in [a, b], \\ V(a) = h \end{cases}$$

and $\nabla_{\dot\gamma}$ is the covariant derivative along γ. The parallel transport is a linear isometry between $T_{\gamma(a)}M$ and $T_{\gamma(b)}M$.

The parallel transport in the finite dimensional Stiefel manifolds $\mathbf{St}(p,\mathbb{R}^n)$ is described in Sec. 2.2.3 in [15]. Given a $n\times p$ orthogonal matrix Y, a tangent vector Δ at Y is represented as a $n\times p$ real matrix such that $Y^T\Delta$ is skew symmetric. Given a curve $Y=Y(t)$ in $\mathbf{St}(p,\mathbb{R}^n)$, the equation for the parallel transport of Δ is

$$\dot\Delta = -Y(\dot Y^T\Delta + \Delta^T\dot Y)/2 \tag{3.37}$$

by Eqn. (2.16) in [15]. According to [15], no closed form solution is known for this equation, even for the case when Y is a geodesic.

The equation for the parallel transport in $\mathbf{St}(2,\mathbb{L}^2)$ can be easily adapted from the equation above. As for the case of geodesics, we can reduce the problem of computing the parallel transport in $\mathbf{St}(2,\mathbb{L}^2)$ along a geodesic, to a computation in a finite dimensional Stiefel manifold. We first note this proposition.

Proposition 3.14.

- *Suppose that $Y=Y(t)$ is a curve, and that v is a vector that is orthogonal to all columns in $Y(t)$, then it is also orthogonal to all columns in $\dot\Delta(t)$.*
- *If Δ is a constant matrix and all its columns are orthogonal to all the columns of $Y(t)$ (for all t), then Δ satisfies (3.37).*

This proposition is stated for the case of $\mathbf{St}(p,\mathbb{R}^n)$, but easily extends to $\mathbf{St}(p,\mathbb{L}^2)$. So we obtain this simplified method to compute the parallel transport in $\mathbf{St}(2,\mathbb{L}^2)$.

Corollary 3.15. *Suppose that $(e(t),f(t))$ is a geodesic in $\mathbf{St}(2,\mathbb{L}^2)$. Let $\mathcal{B}$ be the base used in Proposition 3.9, let $Y(t)$ be the geodesic expressed in this base, (note that $Y(t)$ is a geodesic in $\mathbf{St}(2,\mathbb{R}^4)$). Suppose that $(b(t),d(t))$ is the parallel transport of $(b(0),d(0))$ along $(e(t),f(t))$. We decompose both $b(t)$ and $d(t)$ in two components*

$$b(t)=\tilde b(t)+\hat b(t) \quad , \quad d(t)=\tilde d(t)+\hat d(t)$$

with $\tilde b$ and $\tilde d$ in the 4 dimensional space spanned by $\mathcal{B}$ and $\hat b,\hat d$ orthogonal to this space. From the previous proposition and uniqueness of solution of the linear first order system of ODE (3.37), we obtain that $\hat b,\hat d$ are constant; if we express $\tilde b,\tilde d$ as the two columns of a matrix Δ, using the base $\mathcal{B}$, then Δ satisfies the equation (3.37) in $\mathbf{St}(2,\mathbb{R}^4)$.

4. Filtering and Prediction for Deforming Shapes.

4.1. Dynamical Model . The geometry in the space of curves described in the previous section gives the foundations for defining dynamical systems on curves. In this section, we show how to construct the simplest possible non-trivial dynamical model. Later in experiments, we show the usefulness of the model. Defining more complex dynamical models is beyond the scope of this paper, which is to develop the tools for which any dynamical model can be defined.

We start by considering a simple “constant-velocity plus perturbation” model for a point moving in $\mathbb{R}^n$

$$\begin{aligned}\mu_k &= \mu_{k-1}+\nu_{k-1}\\ \nu_k &= \nu_{k-1}+\eta_{k-1}\end{aligned} \tag{4.1}$$

where the state is $x_k=(\mu_k,\nu_k)$, η_{k-1} is a noise process, and μ represents the position and ν the velocity. When $\{\eta_k\}$ is a white Gaussian process, this is a discrete-time Brownian motion, or first-order random walk.

We assume that we are given noisy measurements of the first component of the state, i.e.,

$$y_k = \mu_k + \xi_k \tag{4.2}$$

where ξ_k is the measurement noise.

We now generalize the above dynamical model from $\mathbb{R}^n$ to the case of curves. Denote with $\mu_k \in B$ the *deforming contour*, and $\nu_k \in T_{\mu_k}B$ its *velocity* at time k. The state at time k is $x_k = (\mu_k, \nu_k)$. In the Riemannian manifold B we may define the analogous operation to addition, i.e., $\mu_k + \nu_k$, by using the exponential map. Also, since ν_k and ν_{k-1} are not in the same space (i.e., $\nu_k \in T_{\mu_k}B$ and $\nu_{k-1} \in T_{\mu_{k-1}}B$), the expression $\nu_k = \nu_{k-1} + \eta_{k-1}$ is not defined, and we must transport ν_{k-1} to $T_{\mu_k}B$ via parallel transport.

The "constant-velocity plus perturbation" model in the space of curves becomes

DEFINITION 4.1 (Discrete Brownian Motion of Curves).

$$\mu_k = \exp_{\mu_{k-1}}(\nu_{k-1}) \tag{4.3}$$

$$\nu_k = P_{\mu_{k-1},\mu_k}(\nu_{k-1} + \eta_{k-1}) \tag{4.4}$$

where $x_k = (\mu_k, \nu_k) \in TB$ *is the state,* $\eta_{k-1} \in T_{\mu_{k-1}}B$ *is a* noise process*, and* P_{μ_{k-1},μ_k} *denotes parallel transport along the geodesic connecting* μ_{k-1} *to* μ_k*. Note that the noise process lives in a linear space, where it is easy to define a Gaussian distribution.*

Since the parallel transport is a linear isometry, the equation (4.4) *can be replaced by*

$$\nu_k = P_{\mu_{k-1},\mu_k}(\nu_{k-1}) + \eta_{k-1} \tag{4.5}$$

simply by choosing directly $\eta_{k-1} \in T_{\mu_k}B$*.*

The two models (4.3),(4.4) *and* (4.3),(4.5) *have equivalent descriptive power. The latter model is though easier to implement numerically, since the parallel transport* $P_{\mu_{k-1},\mu_k}(\nu_{k-1})$ *is trivial to compute: it is the parallel transport along a geodesic of its own tangent vector, so it is obtained as* $\dot\gamma(1)$ *where* γ *is the geodesic between* $\gamma(0) = \mu_{k-1}$ *and* $\gamma(1) = \mu_k$*; and* γ *is exactly the geodesic computed in* (4.3)*.*

We will assume that noisy samples of the contour μ_k are available at each time k, for instance from a segmentation scheme from the active contour literature.

DEFINITION 4.2 (Measurement Model).

$$y_k = \exp_{\mu_k}(\xi_k) \tag{4.6}$$

where $\xi_k \in T_{\mu_k}B$ *is the measurement noise.* The measurement is a noisy version of the first component of the state, μ_k. Again, notice that ξ_k lives on a linear space, where a Gaussian distribution can be easily defined.

4.2. Filtering Deforming Shapes. In this section, the goal is to devise a recursive (causal) procedure to estimate the state of the dynamical system, (μ_k, ν_k), i.e., the shape and velocity of a moving object, introduced in the previous section, from measurements y_k obtained from the time-varying image, I_k. We start by reviewing the classical linear finite-dimensional (Luenberger) observer in $\mathbb{R}^n$ [28], then generalize it to the space of curves.

An observer in $\mathbb{R}^n$ for the dynamical system (4.1) and measurement model (4.2) is itself a dynamical model with state $(\hat{\mu}, \hat{\nu})$ that evolves according to two pairs of equations, the *state prediction*

$$\hat{\mu}_{k|k-1} = \hat{\mu}_{k-1|k-1} + \hat{\nu}_{k-1|k-1} \tag{4.7}$$

$$\hat{\nu}_{k|k-1} = \hat{\nu}_{k-1|k-1} \tag{4.8}$$

and the *update*

$$\hat{\mu}_{k|k} = \hat{\mu}_{k|k-1} + K_\mu(y_k - \hat{\mu}_{k|k-1}) \tag{4.9}$$

$$\hat{\nu}_{k|k} = \hat{\nu}_{k|k-1} + K_\nu(y_k - \hat{\mu}_{k|k-1}) \quad . \tag{4.10}$$

Note how the Luenberger observer structure involves a direct effect of the measurement y_k on the state through two components $K_\mu, K_\nu \geq 0$, which are called the *gains* [8]. The gains can be chosen to satisfy some optimality criterion. The weakest requirement, for time-invariant models, is that the error

$$e_k = x_k - \hat{x}_{k|k}$$

between the state estimate and the true state approaches zeros as $k \to +\infty$.

The analogous observer in the case of the dynamical system on the space of curves may take the following form.

Definition 4.3 (Curve Observer). *The prediction is*

$$\hat{\mu}_{k|k-1} = \exp_{\hat{\mu}_{k-1|k-1}}(\hat{\nu}_{k-1|k-1}) \tag{4.11}$$

$$\hat{\nu}_{k|k-1} = P_{\hat{\mu}_{k-1|k-1}, \hat{\mu}_{k|k-1}}(\hat{\nu}_{k-1|k-1}) \tag{4.12}$$

where $\hat{\nu}_{k|k-1} \in T_{\hat{\mu}_{k|k-1}}B$ *and* $P_{\hat{\mu}_{k-1|k-1}, \hat{\mu}_{k|k-1}}$ *denotes parallel transport along the geodesic from* $\hat{\mu}_{k-1|k-1}$ *to* $\hat{\mu}_{k|k-1}$*; again* $P_{\hat{\mu}_{k-1|k-1}, \hat{\mu}_{k|k-1}}(\hat{\nu}_{k-1|k-1})$ *is trivial to compute.*

The general form of the update equations may be expressed as

$$\hat{\mu}_{k|k} = \exp_{\hat{\mu}_{k|k-1}}(K_\mu \log(\hat{\mu}_{k|k-1}, y_k)) \quad , \tag{4.13}$$

$$\hat{\nu}_{k|k} = P_{\hat{\mu}_{k|k-1}, \hat{\mu}_{k|k}}(\hat{\nu}_{k|k-1} + K_\nu \log(\hat{\mu}_{k|k-1}, y_k)) \quad . \tag{4.14}$$

To better understand the above equations (and give meaning to log*), we identify the* update geodesic ζ_k *such that*

$$\begin{aligned} \zeta_k(0) &= \hat{\mu}_{k|k-1} \quad , \\ \dot{\zeta}_k(0) &= \log(\hat{\mu}_{k|k-1}, y_k) \quad , \\ \zeta_k(1) &= y_k \quad , \\ \zeta_k(K_\mu) &= \hat{\mu}_{k|k} \quad ; \end{aligned}$$

where ζ_k *in the interval* $[0,1]$ *is a minimal geodesic. Since* $P_{\hat{\mu}_{k|k-1}, \hat{\mu}_{k|k}}$ *is the parallel transport along this geodesic, then* (4.14) *can be rewritten as*

$$\hat{\nu}_{k|k} = P_{\hat{\mu}_{k|k-1}, \hat{\mu}_{k|k}}(\hat{\nu}_{k|k-1}) + K_\nu \dot{\zeta}_k(K_\mu) \quad . \tag{4.15}$$

[8] In general, the gains can be matrices such as in the Kalman filter, where these matrices are chosen to minimize the expected square error between the state and estimated state when the noise process is chosen to be Gaussian. We choose the simpler case of an isotropic gain that reduces to a scalar since such a case generalizes easily in the infinite dimensional case, which we examine next.

In any case, the update requires parallel-transport of a tangent vector that is not tangent to the geodesic path to be transported along, which entails solving a differential equation numerically. While this is feasible (and not particularly burdensome, as explained in Corollary 3.15) we will consider in this paper only the simplified observer structure where the correction occurs at the velocity level, and therefore $K_\mu = 0$. Then the update takes the form

$$\hat{\mu}_{k|k} = \hat{\mu}_{k|k-1} \tag{4.16}$$

$$\hat{\nu}_{k|k} = \hat{\nu}_{k|k-1} + K_\nu \log(\hat{\mu}_{k|k-1}, y_k). \tag{4.17}$$

The constant $K_\nu > 0$ should be chosen to trade off asymptotic tracking error with convergence speed. Ideally, it should be chosen within bounds that guarantee at least stability of the filtering, or asymptotic decay of prediction error. In practice, stability can only be guaranteed under additional assumptions on the uncertainty process $\{\eta\}$. In this paper we do not examine this issue.

REMARK 4.4. *The contour of the state μ represents the boundary of the object of interest in the image, which is typically a simple closed curve. As we remarked in 3.3.2, for general $\nu \in T_\mu B$ it is not guaranteed that $\exp_\mu(\nu)$ is simple (that, is, immersed and non self-intersecting). However, we have generally observed in the experiments (Section 4.4) that since $\hat{\nu}_{k|k}$ is not chosen arbitrarily (i.e., it is determined by measurements y_k, which are constructed to be simple (see Section 4.3)), $\hat{\mu}_{k|k-1}$ is generally simple. Moreover since we are only performing a one-step prediction* (4.11), *which corresponds to following the geodesic for a short time step, the curve generally remains simple. For more than one step prediction, a more elaborate model is needed to guarantee that the curve remains simple.*

REMARK 4.5. *We discuss the computational complexity of the above observer for numerical computations. Let the curve μ_k be discretized by N sample points. Computing the exponential map* (4.11) *requires first converting to its Stiefel representation* (3.22)*, computing the basis $\mathcal{B}$* (3.25)*, and then applying* (3.24)*. The parallel transport* (4.12) *is automatically computed by the previous formula. Therefore, computing* (4.11), (4.12) *has complexity $O(N)$. Computing* log *in* (4.17) *is more expensive since it requires an iterative procedure (Algorithm 3.11). Each iteration requires the solution of a tridiagonal system (Appendix D), and this can be done in $O(N)$. Thus, the complexity for* (4.17) *is $O(N * P)$ where P is the number of iterations in Algorithm 3.11. Hence, the overall complexity of the curve observer for at each time k is $O(N * P)$.*

4.3. Obtaining Pseudo-Measurements Via Image Segmentation. In this section, we describe the procedure to obtain the pseudo-measurements y_k of the state contour μ_k using the image sequence $I_k : \Omega \subset \mathbb{R}^2 \to \mathbb{R}^+$. We call these pseudo-measurements because what is measured is the irradiant energy impinging on a small area element on the image plane, i.e., the intensity of a pixel. However, for the purpose of this section, we assume that an intermediate process is available that converts these measurements into an ideal, closed, planar simple curve. In practice, implementing such an intermediate process may be rather difficult when not impossible, depending on the photometric, geometric and dynamic characteristics of the scene. This issue goes to the heart of much of low-level vision and is well beyond the scope of this paper. Therefore, we will take this assumption with the due caveats, and for the rest of this section assume that such pseudo-measurements y_k are available and, for simplicity, call *them* "measurements." They are the boundary of two disjoint regions obtained by partitioning the image domain Ω into two regions that have distinctive local statistics (e.g. intensity histograms, spatial and temporal regularized derivatives, etc.). In order to find the partitioning boundary, we minimize an energy $E_{ac}(\cdot; I) : B \to \mathbb{R}$ that depends on an image, I, and is defined on the space of curves, B. The goal of this section is not to show how one constructs such an energy, but rather, given any energy, show how to optimize it via a steepest descent algorithm that is intrinsic to the Riemannian geometry of the space B

the following is redundant as it was already mentioned earlier under the metric $\mathbb{H}$ introduced in Section 3. This is different than the Sobolev metric presented in [51, 52], so we present the computation of the gradient of an energy E_{ac} with respect to the metric $\mathbb{H}$. Indeed, the next proposition shows how one calculates the $\mathbb{H}$ gradient from the usual $\mathbb{L}^2$ gradient of an energy.

PROPOSITION 4.6. *Let $E_{ac} : M \to \mathbb{R}$ and suppose that $f \doteq \nabla_{H^0} E_{ac}(c)$ and $g \doteq \nabla_{\mathbb{H}} E_{ac}(c)$ exist. Then $g = g^t + g^l(c - \overline{c}) + L(c) g^d$ is related to f by the following:*

$$g^t = \overline{f} \tag{4.18}$$

$$g^l = \frac{1}{\lambda_l} \overline{f \cdot (c - \overline{c})} \tag{4.19}$$

$$g^d = \frac{1}{\lambda_d L(c)} \left(\overline{f \cdot (c - \overline{c})}(c - \overline{c}) - \hat{w} + k \right) \tag{4.20}$$

where

$$\begin{array}{llllll} A & \stackrel{def}{=} & (D_s c)(c - \overline{c})^T \quad , & \hat{f}(\sigma) & \stackrel{def}{=} & \int_0^\sigma f(s)\,\mathrm{d}s - \sigma \overline{f} \quad , \\ v & \stackrel{def}{=} & ⨏_c \hat{f} + A\overline{f}\,\mathrm{d}s \quad , & \hat{w}(\sigma) & \stackrel{def}{=} & \int_0^\sigma \hat{f}(s) + A\overline{f}\,\mathrm{d}s - \sigma v \quad , \\ k & \stackrel{def}{=} & ⨏_c \hat{w} + A^T(\hat{f} + A\overline{f} - v)\,\mathrm{d}s & & & \end{array}$$

and the above parameterizations are in arc parameter.

Proof. See Appendix C. ☐

For the experiments in Section 4.4, in order to obtain measurements, we will minimize an energy of the form

$$E_{ac}(c; I) = \int_R F(x; I)\,\mathrm{d}x \tag{4.21}$$

where R is the region enclosed by the simple curve c, $F : \Omega \to \mathbb{R}$ incorporates information from the image I, and $\mathrm{d}x$ is the area measure in Ω. Such energies have been introduced in a number of papers in the active contour literature (e.g. [7, 59, 42, 62]). It can be shown that the H^0 gradient of (4.21) is

$$\nabla_{H^0} E_{ac}(c; I) = F\mathcal{N}, \tag{4.22}$$

where $\mathcal{N}$ is the outward unit normal to the curve c. The $\mathbb{H}$ gradient of E_{ac} in (4.21) may be computed from (4.22) using Proposition 4.6. Therefore, the measurement y_k is obtained by solving the following partial differential equation (PDE):

$$\partial_t C = -\nabla_{\mathbb{H}} E_{ac}(C; I_k) \tag{4.23}$$

$$C(0, \cdot) = \hat{\mu}_{k|k-1}, \tag{4.24}$$

where $C : \mathbb{R}^+ \times \mathbb{S}^1 \to \mathbb{R}^2$. That is, the $\mathbb{H}$ gradient descent is run until convergence using the predicted contour $\hat{\mu}_{k|k-1}$ at time k as the initialization.

Although the techniques constructed in this paper are built for tracking a single object, in order to solve the PDE (4.23) numerically, we use the level set method [40], which naturally allows for topological changes of the underlying curve C. The use of level set methods is beneficial even when the objects of interest do not exhibit topological changes, because a coarse initialization can undergo several topological changes before converging to a simple curve, which affords improved resistance to local minima. This is, of course, based on empirical evidence, as theoretical guarantees for convergence to local minima are hard to come by for the kind of functionals commonly used in image segmentation. When the method converges to multiply connected curves, we choose the component corresponding to a simple curve that has minimal energy according to (4.21) for the measurement y_k. Instead of evolving the curve C, the level set method evolves a Lipschitz function $\Psi : \mathbb{R}^+ \times \Omega \to \mathbb{R}$ such that $\Psi(t, C(t, \cdot)) = 0$, i.e., the zero level set of Ψ is the curve C. The previous equation defines the evolution of Ψ along the level set:

$$\partial_t \Psi(t, x) = -\nabla\Psi(t, x) \cdot G(t, x), \text{ for } x \in C(t, \mathbb{S}^1)$$

where G is an extension of $-\nabla_{\mathbb{H}} E_{ac}$ in a narrowband of $C(t, \cdot)$:

$$G(t, C(t, s)) = -\nabla_{\mathbb{H}} E_{ac}(C; I_k)(s) \text{ for } s \in [0, L] \tag{4.25}$$

$$\nabla\Psi(t, x) \cdot \nabla G(t, x) = 0 \text{ for } x \notin C(t, \mathbb{S}^1). \tag{4.26}$$

The second equation above implies that the value of G at a point $x \notin C(t, \mathbb{S}^1)$ is equal to $G(t, C(t, s))$ where $C(t, s)$ is the point on $C(t, \mathbb{S}^1)$ closest to x. Note that this is the case for x with a small narrowband around $C(t, \mathbb{S}^1)$. More details for the numerical implementation can be found in [51].

4.4. Experiments. In this section we aim to illustrate the general qualitative behavior of the dynamical model that we have constructed, and the ensuing filter. Therefore, we have chosen a very basic segmentation technique to obtain the measurements y_k, by performing an active contour segmentation using the Chan-Vese model [7] and Sobolev active contours [51, 52] with the initialization being the previous state prediction, $\hat{\mu}_{k|k-1}$. At the initial time, the state contour, $\hat{\mu}_{0|0}$, is selected interactively and the state velocity $\hat{\nu}_{0|0}$ is set to zero. Furthermore, we have chosen the gain $K = 0.2$ unless specified otherwise. The red curve in the figures indicates the state prediction contour $\hat{\mu}_{k|k-1}$, the blue arrows indicate the state prediction velocity $\hat{\nu}_{k|k-1}$, and the green curves indicate the measurement y_k all at frame k.

In the first experiment (Fig. 4.1), we track a circle that continuously deforms (by a non-affine deformation) into two joined blobs. The data is corrupted by a full occlusion in frames 6-11 (the sequence ranges from 1-13). In frame 1, we choose the contour initialization to match the circle's boundary. In the top row, we have used a dynamical model and filter on the affine motion parameters of the object as is typical in prior work [22]. In the bottom row, we have used the proposed method, which defines a dynamical model and filters on the space of curves. At the moment of occlusion ($t = 6$), we set the gain $K = 0$ in which case the filter ignores the measurements y_k, and moves according to state dynamics for $t \geq 6$ with the initial velocity $\hat{v}_{6|6}$. When only affine dynamics are considered, the shape of the object evolves towards an ellipse. The dynamical model on arbitrary deformations, on the other hand, correctly extrapolates during the occlusion and eventually converges to the bi-lobate shape.

In Fig. 4.2 and 4.3, we track a deforming flatworm in the ocean. Fig. 4.2 shows the proposed filtering technique applied to the sequence. The experiment demonstrates

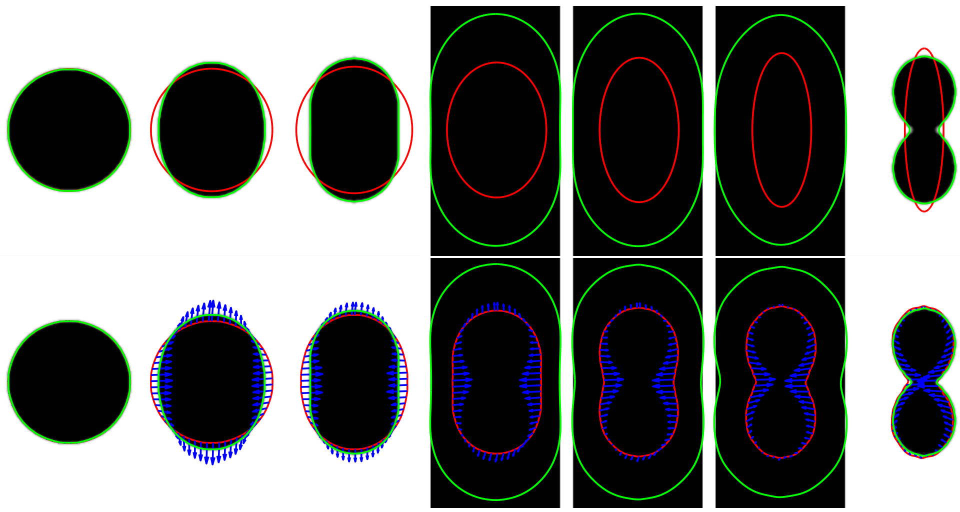

Fig. 4.1. *Tracking a synthetic deforming circle through a total occlusion. This experiment demonstrates the need for the dynamical model that extrapolates shape. In the first few frames, where there is no occlusion, the image segmentation (green) alone correctly follows the shape evolution. However, when the occlusion appears, the image segmentation is uninformative, and the dynamical model extrapolates the shape (red) and velocity (blue) of the contour (middle frames). A dynamical model with only affine motion [22] (top row) cannot extrapolate the deformation. The infinite-dimensional model (proposed work), on the other hand, correctly predicts the evolution towards a bi-lobate shape. Red: $\hat{\mu}_{k|k-1}$; blue: $\hat{\nu}_{k|k-1}$ and green: y_k.*

that the constant velocity plus perturbation model (whose trajectory is shown in red and blue arrows) does a good job at predicting and extrapolating the boundary and motion of the object. In Fig. 4.2, we compare our proposed model to a simple frame-by-frame segmentation (e.g., no filtering in time) [37], and a filtering strategy that only filters and models on the affine motion [22]. As one can see from the figure, the proposed model yields a more accurate track than the affine motion model. In contrast, the affine model predicts a contour that is far enough from the desired local minimum that the measurement "leaks" into portions of the background with similar intensity.

In Figure 4.4, we track a contracting heart chamber from Magnetic Resonance Images (MRI) and compare the results of frame-by-frame segmentation [37], tracking with an affine motion predictor/estimator [22], and the tracking using the proposed prediction/estimation scheme on both shape and motion. As can be seen, a better prediction by the proposed model leads to more accurate measurements that prevents leaking (to a large extent) to the irrelevant chamber. Note that the gradient descent of the image-based energy was run for the same number of fixed iterations for all three tracking procedures.

5. Conclusion. We have introduced a new geometric metric in the space of closed planar curves that decomposes the space into three intuitive components. This decomposition, we have shown, has particular relevance in the tracking problem for computer vision. We have introduced a filtering and prediction scheme on the infinite-dimensional space of shapes, defined as simple, closed planar contours undergoing general diffeomorphisms. Previous work has either attempted to "separate" the "motion" (a finite-dimensional group) from the "deformation", and defined observers for

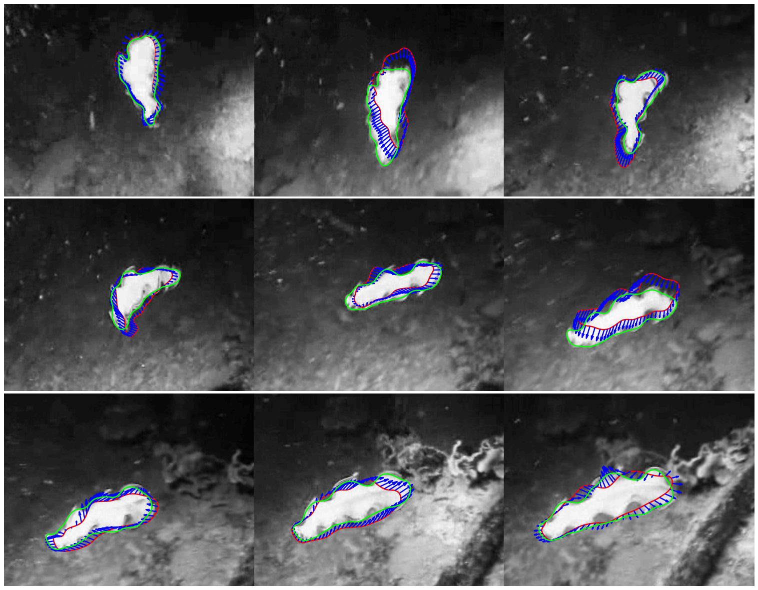

FIG. 4.2. *Tracking a flatworm (left to right, top to bottom) using the proposed filtering technique: the red curve is $\hat{\mu}_{k|k-1}$, the blue arrows are $\hat{\nu}_{k|k-1}$, and the green curve is the measurement y_k. This experiment demonstrates the dynamics of the contour and deformation under the constant velocity plus perturbation model, which correctly models the dynamics of the flatworm.*

dynamical models on the finite-dimensional motion parameters, or has restricted the set of allowable deformations to finitely-parametrized classes, for instance obtained from manually obtained training data. The problem with the former approach is that it fails to predict deformations; as an object undergoes an occlusion, the tracker can extrapolate its affine motion, but not its deformation. We have shown that predicting deformations allows us to significantly decrease prediction error. The problem with the latter approach is that it requires having training data available for the classes of objects and deformations that one wishes to track. While this is realistic for objects like humans walking, it becomes prohibitive when one wants to consider more gaits (limping, running, hopping), or more objects (flatworms, jellyfish, hurricanes) for which training data may not be available.

Deriving a dynamic observer on the space of curves entails the use of Differential and Riemannian geometry, and extends classical results in prediction and filtering theory. We have illustrated the case of (first-order) random walk dynamics, but our approach can be easily extended to any linear dynamics, for instance auto-regressive moving-average models of higher order. This is made possible by the fact that the stochastic processes driving the dynamics are defined on the tangent space to the state-space, which is linear and therefore standard tools from systems theory can be applied, albeit with care because these linear spaces are still infinite-dimensional.

While one may wish to bypass the significant mathematical burden by discretizing the objects of interest at the outset, for instance by using a piecewise linear contour, or a spline or Bezier curve, this introduces difficulties later on. In fact, the location of control points or vertices can move while keeping the data unchanged, which results in an un-observable model, and therefore causes spurious dynamics in the observer. Our approach avoids these representational issues by modeling directly the native

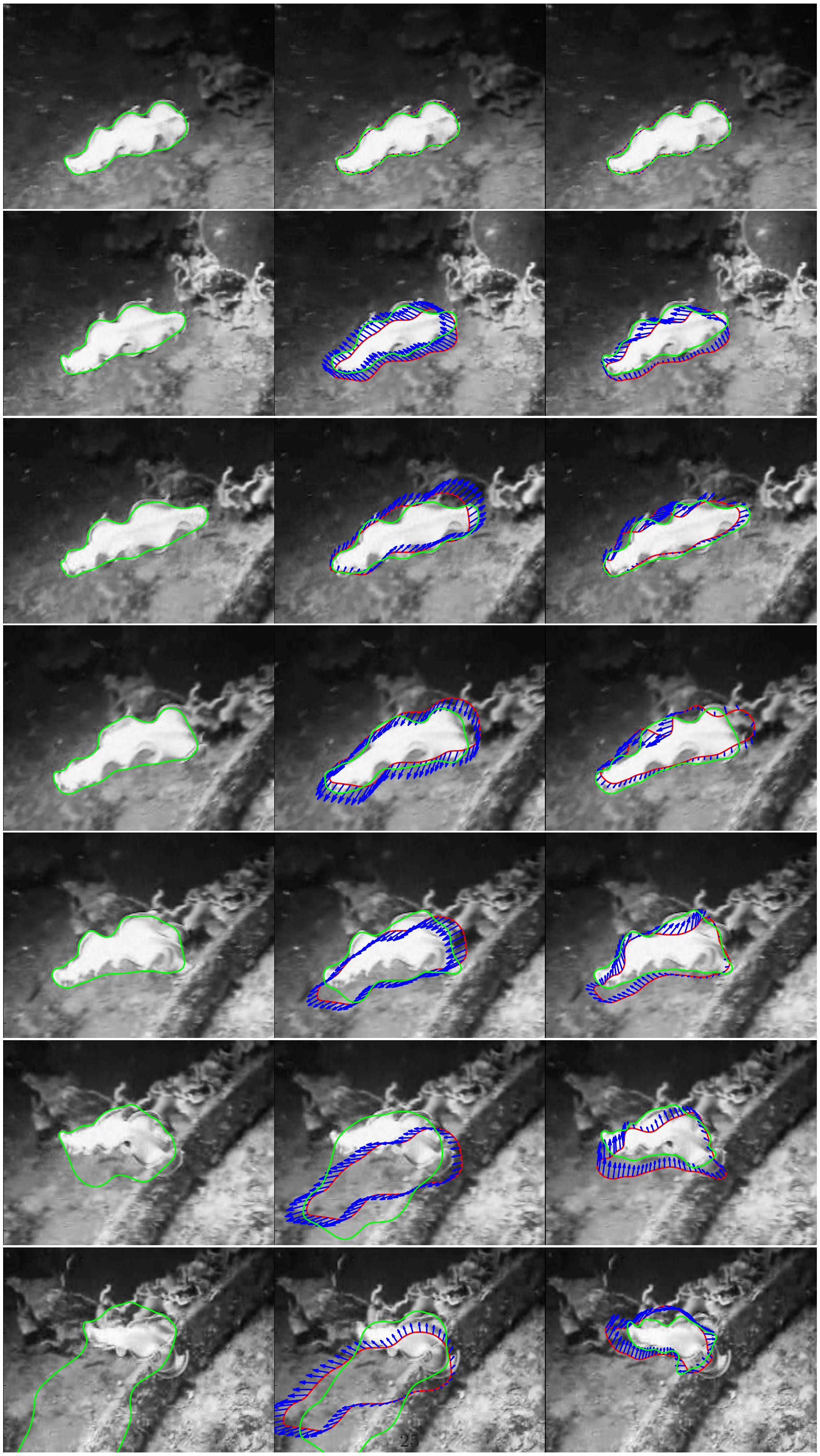

FIG. 4.3. *Comparison between frame-by-frame segmentation, i.e., no dynamics [37] (left), dynamical model only on the motion (scales and translation) [22] in the middle column and dynamical model on both the motion and deformation (proposed work, right column). On the left column it can be seen that the predicted shape fails to adapt to the newly deformed object; on the right column, where both motion and deformation are extrapolated, the object is predicted with far greater accuracy. Red: $\hat{\mu}_{k|k-1}$, blue: $\hat{\nu}_{k|k-1}$, and green: y_k.*

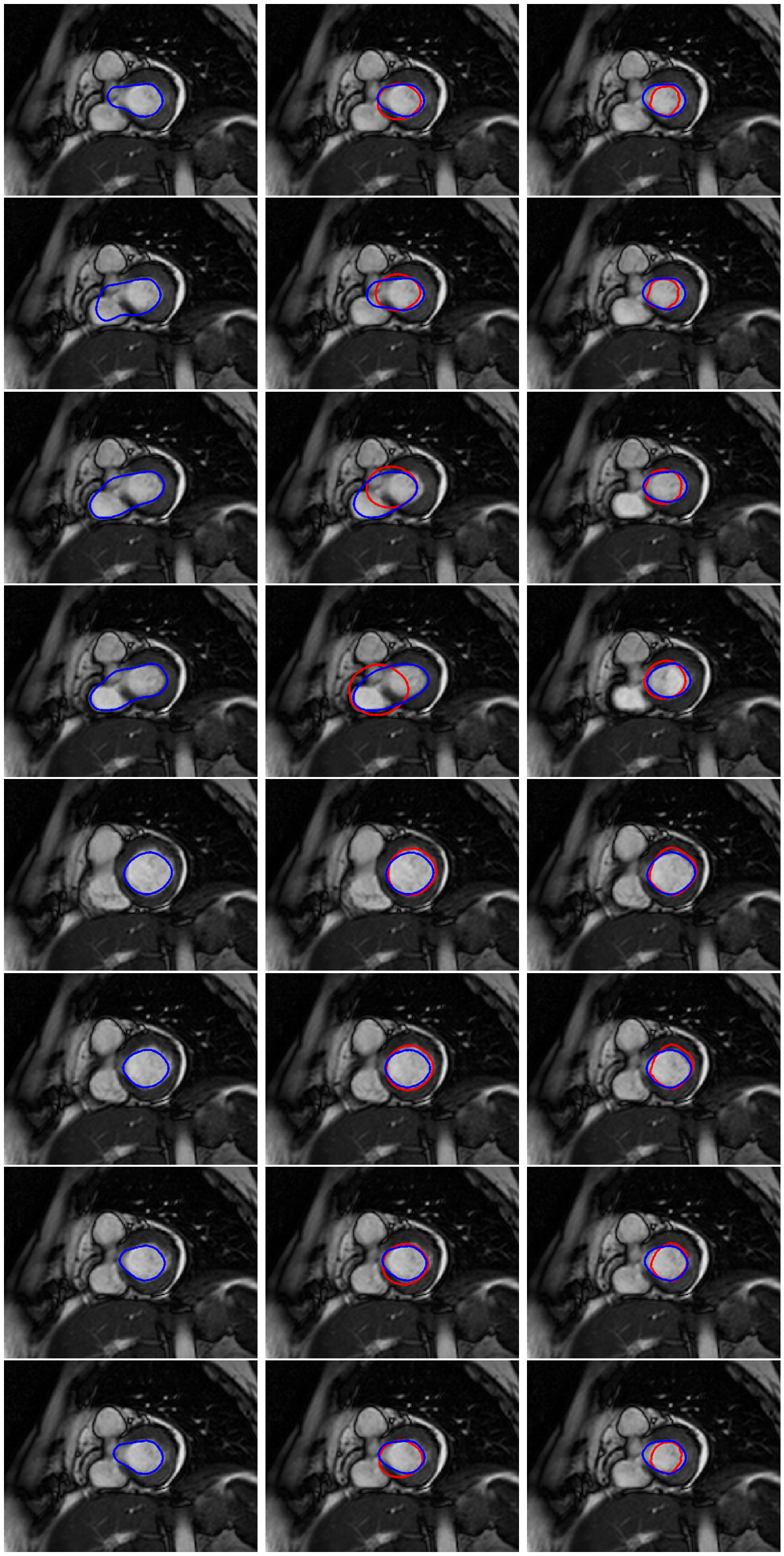

Fig. 4.4. *Tracking a ventricle in a contracting heart from MRI. Left column: frame-by-frame segmentation (no dynamics) [37], middle column: dynamical model on the motion (scales and translation) [22], and right column: dynamical model on both the motion and deformation (proposed work). In both the left and middle columns, the contour leaks into an irrelevant chamber. On the right, because the deformation is predicted, the contour is predicted with greater accuracy (although not perfect) and thus results in better measurements (preventing leaking to a large extent). Red:* $\hat{\mu}_{k|k-1}$, *blue:* y_k.

objects – closed simple planar contours – in the space where they belong, leaving the discretization to the last stage of computation, which is the numerical integration of the partial differential equations implementing the observer. Our approach has been demonstrated on real and synthetic sequences of deforming objects, and shows improvement over the state of the art.

Acknowledgements. This research was funded by AFOSR FA9550-09-1-0427, by NSF grant CCF-0728911, and by `SNS09MENNB` of the Scuola Normale Superiore.

The authors wish to thank Stefano Deiala for his very detailed reading of the manuscript during the preparation of the final draft. His corrections, comments, and many valuable suggestions are greatly appreciated.

Appendix A. Proofs. We first rewrite the metric $\mathbb{H}$ in a form that will be more convenient for the following proofs. Let $P_c h$ be the projector linear operator

$$P_c h \stackrel{\text{def}}{=} h - (D_s c) \fint_c (h \cdot D_s c)\, \mathrm{d}s \ . \tag{A.1}$$

then the three term of the metric $\mathbb{H}$ may be rewritten as

$$\|h\|^2_{\mathbb{H}\text{-t}} = \left| \fint p(h)\, \mathrm{d}s \right|^2 = |D\overline{c}(c;h)|^2 \tag{A.2}$$

$$\|h\|^2_{\mathbb{H}\text{-l}} = \left| \fint_c D_s h \cdot D_s c\, \mathrm{d}s \right|^2 = |D(\log(L(c)))(c;h)|^2 \tag{A.3}$$

$$\begin{aligned} \|h\|^2_{\mathbb{H}\text{-d}} &= L(c)^2 \fint_c |D_s h^d|^2\, \mathrm{d}s = \\ &= \fint_c |P_c(D_s h)|^2\, \mathrm{d}s = \fint_c |D_s h|^2\, \mathrm{d}s - \left(\fint_c D_s h \cdot D_s c\, \mathrm{d}s \right)^2 \ , \end{aligned} \tag{A.4}$$

so that

$$\|h\|^2_{\mathbb{H}} = \|h\|^2_{\mathbb{H}\text{-t}} + \lambda_l \|h\|^2_{\mathbb{H}\text{-l}} + \lambda_d \|h\|^2_{\mathbb{H}\text{-d}} \ .$$

A.1. Proof of Theorem 3.2. We now prove Theorem 3.2.

Proof. Using Hölder's inequality and the fact that $P_c h$ is a projection operator for the metric H^0, we obtain the following three inequalities for the three terms that compose $\mathbb{H}$

$$\begin{aligned} \|h\|^2_{\mathbb{H}\text{-t}} &= |\fint_c h + (c - \overline{c})(D_s h \cdot D_s c)\, \mathrm{d}s|^2 \\ &\leq 2|\fint_c h\, \mathrm{d}s|^2 + 2L(c)^2 \fint_c |D_s h|^2\, \mathrm{d}s \leq \big(2 + \frac{2}{\lambda}\big) \|h\|^2_{\tilde{H}^1} \ ; \\ \|h\|^2_{\mathbb{H}\text{-l}} &\leq \fint_c |D_s h|^2\, \mathrm{d}s \leq \frac{1}{\lambda L(c)^2} \|h\|^2_{\tilde{H}^1} \ ; \\ \|h\|^2_{\mathbb{H}\text{-d}} &\leq \fint_c |D_s h|^2\, \mathrm{d}s \leq \frac{1}{\lambda L(c)^2} \|h\|^2_{\tilde{H}^1} \ . \end{aligned}$$

We then multiply the second by λ_l and the third by λ_d and sum up so that we obtain the inequality

$$\|h\|^2_{\mathbb{H}} \leq \|h\|^2_{\tilde{H}^1} \left(\frac{\lambda_d + \lambda_l}{\lambda L(c)^2} + \big(2 + \frac{2}{\lambda}\big) \right)$$

that entails

$$\|h\|_{\mathbb{H}} \le \|h\|_{\tilde H^1} \frac{1}{a_1}\left(\frac{1}{L(c)}+1\right)$$

for an appropriate small $a_1 > 0$, from which the leftmost thesis of Theorem 3.2 follows. Conversely,

$$\fint_c |D_s h|^2 \,\mathrm{d}s = \fint_c |P_c(D_s h)|^2 \,\mathrm{d}s + \left(\fint_c (D_s h\cdot D_s c)\,\mathrm{d}s\right)^2 = \|h\|^2_{\mathbb{H}\text{-d}} + \|h\|^2_{\mathbb{H}\text{-l}} \tag{A.5}$$

and

$$\begin{aligned} |\fint h\,\mathrm{d}s|^2 &\le 2|\fint_c h + (c-\overline{c})(D_s h\cdot D_s c)\,\mathrm{d}s|^2 + 2|\fint_c (c-\overline{c})(D_s h\cdot D_s c)\,\mathrm{d}s|^2 \le \\ &\le 2\|h\|^2_{\mathbb{H}\text{-t}} + 2L(c)^2\|h\|^2_{\mathbb{H}\text{-l}} \end{aligned} \tag{A.6}$$

so multiplying (A.5) by $\lambda L(c)^2$ and summing with (A.6) yields

$$\|h\|^2_{\tilde H^1} \le \lambda L(c)^2 \|h\|^2_{\mathbb{H}\text{-d}} + (\lambda+2)L(c)^2\|h\|^2_{\mathbb{H}\text{-l}} + 2\|h\|^2_{\mathbb{H}\text{-t}}$$

hence

$$\|h\|_{\tilde H^1} \le \|h\|_{\mathbb{H}} \left(\frac{\lambda L(c)^2}{\lambda_d} + \frac{(\lambda+2)L(c)^2}{\lambda_l} + 2\right)^{1/2} \quad .$$

□

A.2. Proof of Theorem 3.4. We now prove Theorem 3.4.

Proof. The tangent map of (3.12) is

$$\begin{aligned} &\mathbb{R}^2\times\mathbb{R}\times T_{\tilde c}M_d \to T_cM \\ &\qquad h^t, h^l, h^d \mapsto h = h^t + h^l e^l \tilde c + e^l h^d = \\ &\qquad\qquad = h^t + h^l (c-\overline{c}) + L(c) h^d; \end{aligned} \tag{A.7}$$

and the tangent to the inverse (3.13) is

$$\begin{aligned} &T_cM \to \mathbb{R}^2\times\mathbb{R}\times T_{\tilde c}M_d \\ &\qquad h\mapsto h^t = \fint_c h + (c-\overline{c})(D_s h\cdot D_s c)\,\mathrm{d}s, \\ &\qquad\qquad h^l = \fint_c (D_s h\cdot D_s c)\,\mathrm{d}s, \\ &\qquad\qquad h^d = L(c)^{-1}\big(h - h^t - (c-\overline{c})h^l\big) \end{aligned} \tag{A.8}$$

We now use the equalities shown at the beginning of the appendix, and the definition (3.4) and (3.5), and write

$$\|h\|^2_{\mathbb{H}\text{-t}} = \left|\fint_c h + (c-\overline{c})(D_s h\cdot D_s c)\,\mathrm{d}s\right|^2 = |h^t|^2$$

$$\|h\|^2_{\mathbb{H}\text{-l}} = \left(\fint_c (D_s h\cdot D_s c)\,\mathrm{d}s\right)^2 = (h^l)^2 \quad .$$

We now carefully recall that, in the definition of the metric (3.11) on M_d, we are using arc parameter derivatives w.r.t. the curve $\tilde{c}$ and not the curve c; so

$$\begin{aligned}(D_s h^d) &= \frac{\frac{\partial}{\partial\theta} h^d}{|\frac{\partial}{\partial\theta}\tilde{c}|} = \frac{\frac{\partial}{\partial\theta}\big(h - h^t - (c-\overline{c})h^l\big)}{|\frac{\partial}{\partial\theta}c|} = \\ &= \frac{\frac{\partial}{\partial\theta}h - \frac{\partial}{\partial\theta}c h^l}{|\frac{\partial}{\partial\theta}c|} = D_s h - D_s c(\overline{D_s h \cdot D_s c}) = P_c(D_s h) \end{aligned} \tag{A.9}$$

(where P was defined in (A.1)), so that

$$\|h^d\|^2_{M_d} = \int_{\tilde{c}} |D_s h^d|^2 \ \mathrm{d}s = \fint_c |P_c(D_s h)|^2 \, \mathrm{d}s = \|h\|^2_{\mathbb{H}\text{-d}} \quad .$$

We conclude that (3.12) is an isometry. ▯

A.3. Proof of Proposition 3.6. We now prove Proposition 3.6. The following proof is based on classical methods, first applied to Riemannian geometries of immersed curves in [35].

Proof. Let $\mathcal{G}$ be a group that acts on M. Given a curve $c \in M$, and a tangent vector $\xi \in T_e\mathcal{G}$ (where e is the identity in $\mathcal{G}$, and $T_e\mathcal{G}$ is the *Lie algebra* of $\mathcal{G}$), we derive the action, for fixed c and e "moving" in direction ξ; the result of this derivative is a tangent vector $\zeta = \zeta_{\xi,c} \in T_c M$ (depending linearly on ξ). By the Emmy Noether theorem, if the metric is invariant w.r.t. the action of $\mathcal{G}$, and $\gamma(t)$ is a geodesic, then

$$\Big\langle \zeta_{\xi,\gamma(t)}, \dot{\gamma}(t) \Big\rangle_{\gamma(t)} \tag{A.10}$$

is constant in t, for any choice of $\xi \in T_e\mathcal{G}$.

- For the translation group, $\zeta = \xi \in \mathbb{R}^2$, by (A.2)

  $$\langle \xi, \frac{\partial}{\partial t} C \rangle_{\mathbb{H}} = \xi \cdot \frac{\partial}{\partial t}\overline{C}$$

  is constant for any ξ, hence $\frac{\partial}{\partial t}\overline{C}$ is constant. Alternatively, we can use the isometry in Theorem 3.4.
- The *rotation* group is represented by orthonormal matrices; the tangent $T_e\mathcal{G}$ is the set of the antisymmetric matrices $B \in \mathbb{R}^{2\times 2}$, then $\zeta = BC$. We compute

  $$\begin{aligned} &\langle BC, \frac{\partial}{\partial t} C \rangle_{\mathbb{H}\text{-t}} = B\overline{C} \cdot (\frac{\partial}{\partial t}\overline{C}) \\ &\langle BC, \frac{\partial}{\partial t} C \rangle_{\mathbb{H}\text{-l}} = 0 \\ &\langle BC, \frac{\partial}{\partial t} C \rangle_{\mathbb{H}\text{-d}} = \fint_C (BD_s C) \cdot (D_s \frac{\partial}{\partial t} C) \, \mathrm{d}s \quad . \end{aligned}$$

  We also know that $\frac{\partial}{\partial t}\overline{C}$ is a constant, call it v; so

  $$(B\overline{C}) \cdot (\frac{\partial}{\partial t}\overline{C}) = (B\overline{c_0} + tBv) \cdot v = (B\overline{c_0}) \cdot v,$$

  which is constant. By direct computation,

  $$\frac{\partial}{\partial t}(D_s C) = -(D_s \frac{\partial}{\partial t} C \cdot D_s C)(D_s C) + D_s(\frac{\partial}{\partial t} C) \quad ,$$

so we conclude that

$$\frac{1}{\lambda_d}\langle BC, \frac{\partial}{\partial t}C\rangle_{\mathbb{H}} = \fint_C (BD_sC)\cdot(D_s\frac{\partial}{\partial t}C)\,\mathrm{d}s = \fint_C (BD_sC)\cdot(\frac{\partial}{\partial t}D_sC)\,\mathrm{d}s$$

and that these are constant in t.

- The *reparameterization* group is $\mathcal{G} = \mathrm{Diff}(S^1)$; the action is the composition $\phi, c \mapsto c\circ\phi$; a tangent vector in $T_e\mathcal{G}$ is a scalar field $\xi : S^1 \to \mathbb{R}$; we in the end have that

$$\zeta(\theta) = \xi(\theta)c'(\theta)$$

(where $c' = \frac{\partial}{\partial\theta}c$) or

$$\zeta(\theta) = f(\theta)D_sc(\theta)$$

that is, ζ is a generic vector field parallel to the curve. We compute

$$\langle fD_sC, \frac{\partial}{\partial t}C\rangle_{\mathbb{H}\text{-t}} = 0, \quad \langle fD_sC, \frac{\partial}{\partial t}C\rangle_{\mathbb{H}\text{-l}} = 0$$

from (A.2),(A.3); while

$$\begin{aligned}\langle fD_sC, \frac{\partial}{\partial t}C\rangle_{\mathbb{H}\text{-d}} &= \fint_C (D_s(fD_sC))\cdot(D_s\frac{\partial}{\partial t}C)\,\mathrm{d}s \\ &\quad - \fint (D_s(fD_sC))\cdot D_sC\,\mathrm{d}s \fint (D_sC)\cdot(D_s\frac{\partial}{\partial t}C)\,\mathrm{d}s \\ &= -\fint_C (fD_sC)\cdot(D_s^2\frac{\partial}{\partial t}C)\,\mathrm{d}s \\ &\quad - \fint (fD_sC)\cdot D_s^2C\,\mathrm{d}s \fint (D_s^2C)\cdot(\frac{\partial}{\partial t}C)\,\mathrm{d}s \\ &= -\fint_C f(D_sC)\cdot(D_s^2\frac{\partial}{\partial t}C)\,\mathrm{d}s\end{aligned}$$

since $(D_sC)\cdot(D_s^2C) = 0$.

For the rescaling group, we cannot use Emmy Noether's Theorem directly, since the metric $\mathbb{H}$ is not rescaling invariant as a whole. The result is then a consequence of Theorem 3.4. ∎

Appendix B. Fast Algorithm for Matrix Exponential Derivatives. In this appendix, we derive a fast method for computing

$$D(\exp X)(X; Z) = \int_0^1 \exp(tX)Z\exp((1-t)X)\,\mathrm{d}t.$$

Since $D(\exp X)(X;\cdot)$ is a linear operator acting on Z, we have

$$D(\exp X)(X;Z) = \sum_{ij} z_{ij}\int_0^1 \exp(tX)\Delta_{ij}\exp((1-t)X)\,\mathrm{d}t$$

where $z_{i,j}$ are the components of the matrix Z and Δ_{ij} is the $n\times n$-matrix of components

$$(\Delta_{ij})_{kl} = \begin{cases}1 & (k,l) = (i,j)\\ 0 & (k,l)\neq(i,j)\end{cases}.$$

Noting that $B\Delta_{ij}C = B_{\cdot,i}C_{j,\cdot}$ where $B_{\cdot,i}$ (column vector) denotes column i of B, and $C_{j,\cdot}$ (row vector) denotes row j of C, we have that

$$D(\exp X)(X;Z) = \sum_{ij} z_{ij} \int_0^1 (\exp(tX))_{\cdot,i} (\exp((1-t)X))_{j,\cdot} \, \mathrm{d}t.$$

Note that $(B_{\cdot,i}C_{j,\cdot})_{kl} = (B \otimes C)_{j+n(k-1),(i-1)n+l}$ where $i,j,k,l \in \{1,\dots,n\}$, n is the dimension of X, and $\otimes$ denotes the Kronecker product. Therefore,

$$(D(\exp X)(X;Z))_{kl} = \sum_{ij} z_{ij} \left(\int_0^1 \exp(tX) \otimes \exp((1-t)X) \, \mathrm{d}t \right)_{j+n(k-1),(i-1)n+l} \tag{B.1}$$

We now give a fast method to compute the integral in (B.1). Note that

$$\begin{aligned} \int_0^1 \exp(tX) \otimes \exp((1-t)X) \, \mathrm{d}t &= \int_0^{\frac{1}{2}} \exp(tX) \otimes [\exp((1/2-t)X)\exp(X/2)] \, \mathrm{d}t \\ &\quad + \int_{\frac{1}{2}}^1 [\exp(X/2)\exp((t-1/2)X)] \otimes \exp((1-t)X) \, \mathrm{d}t \\ &= \mathcal{I}_{1/2}(\mathrm{Id}_{n\times n} \otimes \exp(X/2)) + (\exp(X/2) \otimes \mathrm{Id}_{n\times n})\mathcal{I}_{1/2} \end{aligned}$$

where we define

$$\mathcal{I}_{1/2^k} = \int_0^{\frac{1}{2^k}} \exp(tX) \otimes \exp((1/2^k - t)X) \, \mathrm{d}t. \tag{B.2}$$

Analogous to the computation above, we find

$$\mathcal{I}_{1/2^k} = \mathcal{I}_{1/2^{k+1}}(\mathrm{Id}_{n\times n} \otimes \exp(X/2^{k+1})) + (\exp(X/2^{k+1}) \otimes \mathrm{Id}_{n\times n})\mathcal{I}_{1/2^{k+1}}. \tag{B.3}$$

Therefore, given an integer m, we may compute $\mathcal{I}_1$ recursively using the formula (B.3) m times, and $\mathcal{I}_{1/2^m}$ can be approximated using a Riemann sum or any other numerical integration method.

The technique above resembles the Fast Fourier Transform algorithm and is similar to a technique found in [55].

Appendix C. Computing the $\mathbb{H}$ Gradient of Energies.

In this appendix, we compute the gradient of an energy $E_{ac} : M \to \mathbb{R}$ with respect to the $\mathbb{H}$ metric in terms of the H^0 metric. By definition of gradient, we have that

$$DE_{ac}(c;h) = \langle h, \nabla_{\mathbb{H}} E \rangle_{\mathbb{H}} = \langle h, \nabla_{H^0} E \rangle_{H^0}, \ \forall\, h \in T_cM. \tag{C.1}$$

Therefore, we solve

$$⨍_c h \cdot f \, \mathrm{d}s = h^t \cdot g^t + \lambda_l h^l g^l + \lambda_d L(c)^2 ⨍_c D_s h^d \cdot D_s g^d \, \mathrm{d}s,$$

where $f \stackrel{\text{def}}{=} \nabla_{H^0} E$ and $g \stackrel{\text{def}}{=} \nabla_{\mathbb{H}} E$. We set for convenience

$$A = (D_s c)(c - \overline{c})^T \quad ;$$

$A = A(s)$ is a 2×2 matrix field along c; note that

$$h^t = D(\overline{c})(c;h) = ⨍ h - (D_s A^T) h \, \mathrm{d}s \quad .$$

One can show that

$$h^t \cdot g^t = \fint_c h \cdot \left[g^t - (D_s A) g^t\right] \, \mathrm{d}s$$
$$h^l g^l = -\fint_c h \cdot (g^l D_s^2 c) \, \mathrm{d}s$$
$$\fint_c D_s h^d \cdot D_s g^d \, \mathrm{d}s = -\frac{1}{L(c)} \fint_c h \cdot D_s^2 g^d \, \mathrm{d}s \quad .$$

So we must solve for g (i.e., the components g^t, g^l, and g^d of g) in

$$f = [\mathrm{Id} - D_s A] \, g^t - \lambda_l g^l D_s^2 c - \lambda_d L(c) D_s^2 g^d.$$

It is clear that $g^t = \overline{f}$ and noting that g^d does not change the length, we have that

$$\overline{f \cdot (c - \overline{c})} = -\overline{[(D_s A) g^t] \cdot (c - \overline{c})} + \lambda_l g^l = \lambda_l g^l, \tag{C.2}$$

which verifies (4.19). Eventually we obtain the equation

$$-\lambda_l g^l D_s^2 c - (f - \overline{f}) - (D_s A) \overline{f} = \lambda_d L(c) D_s^2 g^d \tag{C.3}$$

We note that the LHS has zero integral along the curve, so we integrate both sides to obtain

$$-\lambda_l g^l D_s c - \hat{f} - A \overline{f} + v = \lambda_d L(c) D_s g^d \tag{C.4}$$

where $\hat{f}(\sigma) \stackrel{\text{def}}{=} \int_0^\sigma (f(s) - \overline{f}) \, \mathrm{d}s$; the above identity is determined up to the constant $v \in \mathbb{R}^2$. Since the RHS of (C.4) has zero average on the curve, this forces the choice of v, that will be

$$v \stackrel{\text{def}}{=} \fint_c \hat{f} + A \overline{f} \, \mathrm{d}s \quad . \tag{C.5}$$

We let then $w \stackrel{\text{def}}{=} \hat{f} + A \overline{f} - v$ and rewrite (C.4) as

$$-\lambda_l g^l D_s c - w = \lambda_d L(c) D_s g^d \quad , \tag{C.6}$$

where both LHS and RHS have zero average.

To solve the above equation (C.6) for g^d, we now integrate once again, and obtain

$$-\lambda_l g^l (c - \overline{c}) - \hat{w} + k = \lambda_d L(c) g^d \quad . \tag{C.7}$$

where $\hat{w}(\sigma) \stackrel{\text{def}}{=} \int_0^\sigma w(s) \, \mathrm{d}s$, and once again the identity is determined up to the constant $k \in \mathbb{R}^2$. The constant k is obtained by imposing that $(g^d)^t = 0$, that is, g^d does not move the centroid of the curve.[9]

Appendix D. Discretization of (3.36)**.** We discretize (3.36) to solve for the vertical component of $(\delta e, \delta f) \in T_{(e,f)} \mathbf{St}(2, C^\infty)$. Let $e_i, f_i, \delta e_i, \delta f_i$ $(1 \le i \le N)$ be uniform samplings of $e, f, \delta e, \delta f : \mathbb{S}^1 \to \mathbb{R}$. Set

$$e_0 = \pm e_N, f_0 = \pm f_N, \delta e_0 = \pm \delta e_N, \delta f_0 = \pm \delta f_N$$
$$e_{N+1} = \pm e_1, f_{N+1} = \pm f_1, \delta e_{N+1} = \pm \delta e_1, \delta f_{N+1} = \pm \delta f_1;$$

[9]The other identity $(g^d)^l = \int_c D_s g^d \cdot D^s c \, \mathrm{d}s = 0$ is true regardless of the choice of k and v, and is verified by the identity (C.4).

one chooses + or − if the curve is of even or odd winding number, respectively. Define b_I, c_i, d_i, g_i $(1 \le i \le N)$ as

$$b_i = -\frac{1}{2}[\delta e_i(e_{i+1} - e_{i-1}) - e_i(\delta e_{i+1} - \delta e_{i-1}) + \delta f_i(f_{i+1} - f_{i-1}) - f_i(\delta f_{i+1} - \delta f_{i-1})]$$

$$c_i = \frac{1}{2}(e_i^2 + f_i^2)$$

$$d_i = \frac{1}{2}[e_i(e_{i+1} - e_{i-1}) + f_i(f_{i+1} - f_{i-1})]$$

$$g_i = \frac{1}{2}\left[e_i(e_{i+1} - 2e_i + e_{i-1}) - \frac{1}{2}(e_{i+1} - e_{i-1})^2 \right.$$
$$\left. + f_i(f_{i+1} - 2f_i + f_{i-1}) - \frac{1}{2}(f_{i+1} - f_{i-1})^2\right]$$

Let $A = (a_{ij})$ where $1 \le i, j \le N$. Set for $1 \le i, j \le N$

$$a_{ii} = -c_i + g_i,\ a_{i(i-1)} = c_i - d_i,\ a_{i(i+1)} = c_i + d_i,\ a_{ij} = 0 \text{ for } j - 1 > i > j + 1$$

and $B = (b_i)$. Note $a_{i0} := a_{iN}, a_{i(N+1)} := a_{i0}$. Then if $x = (\beta_i)$ is a sampling of β in (3.36), then $Ax = B$.

REFERENCES

[1] M. F. Beg, M. I. Miller, A. Trouvé, and L. Younes. Computing large deformation metric mappings via geodesic flows of diffeomorphisms. *International Journal of Computer Vision*, 61(2):139–157, 2005.

[2] A. Blake and R. Brockett. On snakes and estimation theory. In *IEEE CDC*, 1994.

[3] A. Bronstein, M. Bronstein, and R. Kimmel. Calculus of non-rigid surfaces for geometry and texture manipulation. *IEEE Trans. Vis. Comp. Graphics*, 13(5):902–913, 2007.

[4] V. Caselles, F. Catte, T. Coll, and F. Dibos. A geometric model for edge detection. *Num. Mathematik*, 66:1–31, 1993.

[5] V. Caselles, R. Kimmel, and G. Sapiro. Geodesic active contours. In *Proceedings of the IEEE Int. Conf. on Computer Vision*, pages 694–699, Cambridge, MA, USA, June 1995.

[6] V. Cervera, F. Mascaró, and P. W. Michor. The action of the diffeomorphism group on the space of immersions. *Differential Geom. Appl.*, 1(4):391–401, 1991.

[7] T. Chan and L. Vese. Active contours without edges. *IEEE Transactions on Image Processing*, 10(2):266–277, February 2001.

[8] G. Charpiat, O. D. Faugeras, and R. Keriven. Approximations of shape metrics and application to shape warping and empirical shape statistics. *Foundations of Computational Mathematics*, 5(1):1–58, 2005.

[9] G. Charpiat, R. Keriven, J. Pons, and O. Faugeras. Designing spatially coherent minimizing flows for variational problems baseed on active contours. In *ICCV*, 2005.

[10] G. Charpiat, P. Maurel, J.-P. Pons, R. Keriven, and O. Faugeras. Generalized gradients: Priors on minimization flows. *International Journal of Computer Vision*, 2007.

[11] D. Cremers. Nonlinear dynamical shape priors for level set segmentation. In *CVPR*. IEEE Computer Society, 2007.

[12] D. Cremers and S. Soatto. Motion competition: A variational approach to piecewise parametric motion segmentation. *International Journal of Computer Vision*, 62(3):249–265, 2004.

[13] M. Delfour and J. P. Zolésio. Shape identification via metrics constructed from the oriented distance function. *Control and Cybernetics*, 34(1):137–164, 2005.

[14] M. do Carmo. *Riemannian Geometry*. Birkhäuser Boston, 1992.

[15] A. Edelman, T. A. Arias, and S. T. Smith. The geometry of algorithms with orthogonality constraints. *SIAM J. Matrix Anal. Appl.*, 20:303–353, 1998.

[16] R. Goldenberg, R. Kimmel, E. Rivlin, and M. Rudzsky. Fast geodesic active contours. *IEEE Transactions on Image Processing*, 10(10):1467–1475, 2001.

[17] C. Gosch, K. Fundana, A. Heyden, and C. Schnörr. View point tracking of rigid objects based on shape sub-manifolds. In *ECCV*, pages 251–263, 2008.

[18] J. Grabowski. Derivative of the exponential mapping for infinite-dimensional Lie groups. *Ann. Global Anal. Geom.*, 11(3):213–220, 1993.

[19] R. S. Hamilton. The inverse function theorem of Nash and Moser. *Bull. Amer. Math. Soc. (N.S.)*, 7(1):65–222, 1982.
[20] B. K. P. Horn and B. G. Schunck. Determining optical flow. *Artif. Intell.*, 17(1-3):185–203, 1981.
[21] M. Isard and A. Blake. Condensation – conditional density propagation for visual tracking. *IJCV*, 1(29):5–28, 1998.
[22] J. Jackson, A. Yezzi, and S. Soatto. Tracking deformable moving objects under severe occulsions. In *IEEE Conference on Decision and Control*, Dec. 2004.
[23] M. Kass, A. Witkin, and D. Terzopoulos. Snakes: Active contour models. *International Journal of Computer Vision*, 1:321–331, 1987.
[24] D. G. Kendall. Shape manifolds, procrustean metrics and complex projective spaces. *Bull. London Math. Soc., 16*, 16, 1984.
[25] S. Kichenassamy, A. Kumar, P. Olver, A. Tannenbaum, and A. Yezzi. Gradient flows and geometric active contour models. In *Proceedings of the IEEE Int. Conf. on Computer Vision*, pages 810–815, 1995.
[26] M. Kilian, N. Mitra, and H. Pottmann. Geometric modeling in shape space. *ACM Transactions on Graphics*, 26(3):64, 2007.
[27] S. Lang. *Fundamentals of Differential Geometry.* Springer-Verlag, 1999.
[28] D. Luenberger. Observing the state of a linear system. *IEEE Transactions on Military Electronics*, 8(2):74–80, 1964.
[29] R. Malladi, J. Sethian, and B. Vemuri. Shape modeling with front propagation: a level set approach. *IEEE Transactions on Pattern Analysis and Machine Intelligence*, (17):158–175, 1995.
[30] K. V. Mardia and I. L. Dryden. Shape distributions for landmark data. *Adv. Appl. Prob.*, 21(4):742–755, 1989.
[31] R. Mathias. Evaluating the frechet derivative of the matrix exponential. *Numerische Mathematik*, 63:213–226, 1992.
[32] A. Mennucci, A. Yezzi, and G. Sundaramoorthi. Properties of Sobolev Active Contours. *Interf. Free Bound.*, 10:423–445, 2008.
[33] P. Michor and D. Mumford. Riemannian geometries on the space of plane curves. *J. Eur. Math. Soc.*, 8:1–48, 2006.
[34] P. W. Michor and D. Mumford. Vanishing geodesic distance on spaces of submanifolds and diffeomorphisms. *Documenta Math.*, 10:217–245, 2005.
[35] P. W. Michor and D. Mumford. An overview of the Riemannian metrics on spaces of curves using the Hamiltonian approach. *Applied and Computational Harmonic Analysis*, 23:76–113, 2007.
[36] W. Mio and A. Srivastava. Elastic-string models for representation and analysis of planar shapes. In *CVPR (2)*, pages 10–15, 2004.
[37] M. Moelich and T. Chan. Tracking objects with the chan-vese algorithm. Technical report, UCLA, 2003.
[38] D. Mumford and J. Shah. Optimal approximations by piecewise smooth functions and associated variational problems. *Comm. Pure Appl. Math.*, 42:577–685, 1989.
[39] M. Niethammer, P. A. Vela, and A. Tannenbaum. Geometric observers for dynamically evolving curves. *IEEE Trans. Pattern Anal. Mach. Intell.*, 30(6):1093–1108, 2008.
[40] S. Osher and J. Sethian. Fronts propagating with curvature-dependent speed: algorithms based on the Hamilton-Jacobi equations. *J. Comp. Physics*, 79:12–49, 1988.
[41] N. Papadakis and E. Mémin. A variational technique for time consistent tracking of curves and motion. *J. Mathematical Imaging and Vision*, 31(1):81–103, 2008.
[42] N. Paragios and R. Deriche. Geodesic active regions: a new paradigm to deal with frame partition problems in computer vision. *International Journal of Visual Communication and Image Representation, Special Issue on Partial Differential Equations in Image Processing, Computer Vision and Computer Graphics*, 13(2):249–268, June 2002.
[43] N. Peterfreund. The velocity snake: Deformable contour for tracking in spatio-velocity space. *Computer Vision and Image Understanding*, 73(3):346–356, 1999.
[44] Y. Rathi, N. Vaswani, A. Tannenbaum, and A. Yezzi. Particle filtering for geometric active contours and application to tracking deforming objects. In *IEEE CVPR*, 2005.
[45] R. Ronfard. Region based strategies for active contour models. *International Journal of Computer Vision*, 13(2):229–251, October 1994.
[46] M. Rumpf and B. Wirth. A nonlinear elastic shape averaging approach. *SIAM Journal on Imaging Sciences*, 2(3):800–833, 2009.
[47] S. Soatto and A. J. Yezzi. DEFORMOTION: Deforming motion, shape average and the joint registration and segmentation of images. In *ECCV (3)*, pages 32–57, 2002.
[48] G. Sundaramoorthi, A. Mennucci, S. Soatto, and A. Yezzi. Tracking deforming objects by filtering and prediction in the space of curves. In *Conference on Decision and Control*, December 2009.

[49] G. Sundaramoorthi, A. Yezzi, and A. Mennucci. Sobolev active contours. In *VLSM*, pages 109–120, 2005.

[50] G. Sundaramoorthi, A. Yezzi, A. Mennucci, and G. Sapiro. New possibilities with Sobolev active contours. *Intn. Journ. Computer Vision*, 2008.

[51] G. Sundaramoorthi, A. J. Yezzi, and A. Mennucci. Sobolev Active Contours. *International Journal of Computer Vision*, 73(3):345–366, 2007.

[52] G. Sundaramoorthi, A. J. Yezzi, and A. Mennucci. Coarse-to-fine segmentation and tracking using Sobolev Active Contours. *IEEE Trans. Pattern Anal. Mach. Intell.*, 30(5):851–864, 2008.

[53] D. Terzopoulos and R. Szeliski. *Active Vision*, chapter Tracking with Kalman Snakes. MIT Press, 1992.

[54] N. Vaswani, Y. Rathi, A. Yezzi, and A. Tannenbaum. Pf-mt with an interpolation effective basis for tracking local contour deformations. *IEEE Trans. on Image Processing*, 2008.

[55] C. Wasshuber. *Computational Single-Electronics*. Springer, 2001.

[56] B. Wirth, L. Bar, M. Rumpf, and G. Sapiro. Geodesics in shape space via variational time discretization. In *EMMCVPR*, 2009.

[57] A. Yezzi and A. Mennucci. Metrics in the space of curves. *arXiv*, 2004.

[58] A. Yezzi and A. Mennucci. Conformal metrics and true "gradient flows" for curves. In *International Conference on Computer Vision (ICCV05)*, pages 913–919, 2005.

[59] A. Yezzi, A. Tsai, and A. Willsky. A statistical approach to snakes for bimodal and trimodal imagery. In *Int. Conf. on Computer Vision*, pages 898–903, October 1999.

[60] L. Younes. Computable elastic distances between shapes. *SIAM J. Appl. Math.*, 58(2):565–586, 1998.

[61] L. Younes, P. W. Michor, J. Shah, and D. Mumford. A metric on shape space with explicit geodesics. *Rend. Lincei Mat. Appl.*, 9:25–57, 2008.

[62] S. C. Zhu, T. S. Lee, and A. L. Yuille. Region competition: Unifying snakes, region growing, energy/bayes/ MDL for multi-band image segmentation. In *ICCV*, pages 416–, 1995.